Geochemistry Geophysics Geosystems G3
AN ELECTRONIC JOURNAL OF THE EARTH SCIENCES
Published by AGU and the Geochemical Society

Review
Volume 7, Number 10
11 October 2006
Q10N05, doi:10.1029/2006GC001284
ISSN: 1525-2027

Size sorting in marine muds: Processes, pitfalls, and prospects for paleoflow-speed proxies

I. N. McCave
Godwin Laboratory for Palaeoclimate Research, Department of Earth Sciences, University of Cambridge, Downing Street, Cambridge CB2 3EQ, UK (mccave@esc.cam.ac.uk)

I. R. Hall
School of Earth, Ocean and Planetary Sciences, Cardiff University, Main Building, Park Place, Cardiff CF10 3YE, UK

[1] The basis for, and use of, fine grain size parameters for inference of paleoflow speeds is reviewed here. The basis resides in data on deposited sediment taken in conjunction with flow speed measurements in the field, experimental data on suspended sediment transport and deposition, and theoretical treatments of the generation of size distributions of deposits from suspension controlled by particle settling velocity and flow speed. In the deep sea, sorting events occur under resuspension/deposition events in benthic storms. At flow speeds below 10–15 cm s^{-1}, size in the noncohesive "sortable silt" (10–63 μm) range is controlled by selective deposition, whereas above that range, removal of finer material by winnowing also plays a role. The best particle size instruments to measure a flow speed–related grain size employ the settling velocity method, while laser diffraction sizers can yield misleading results because of particle shape effects. Potential problems, including source effects, downslope supply on continental margins, spatial variability of flow over bedforms, and influence of ice-rafted detritus, are examined. A number of studies using the sortable silt flow speed proxy are reviewed, and inverse modeling of grain size distributions is examined. Outstanding problems are that corroboration is sparse because almost no studies have yet used the full range of proxies for flow rate and water mass identification and that the sortable silt mean size is not yet properly calibrated in terms of flow speed.

Components: 21,393 words, 24 figures.

Keywords: sortable silt; grain size; paleocurrent; flow speed; ocean circulation; contourite; sediment drift.

Index Terms: 3022 Marine Geology and Geophysics: Marine sediments: processes and transport; 4576 Oceanography: Physical: Western boundary currents; 4962 Paleoceanography: Thermohaline.

Received 15 March 2006; **Revised** 30 June 2006; **Accepted** 7 August 2006; **Published** 11 October 2006.

McCave, I. N., and I. R. Hall (2006), Size sorting in marine muds: Processes, pitfalls, and prospects for paleoflow-speed proxies, *Geochem. Geophys. Geosyst.*, *7*, Q10N05, doi:10.1029/2006GC001284.

Theme: Past Ocean Circulation
Guest Editors: Jean Lynch-Stieglitz, Catherine Kissel, and Olivier Marchal

1. Introduction

[2] Recent years have seen extensive work on development and application of a proxy for the speed of deep-sea bottom currents because this is an essential physical oceanographic variable. In modern physical oceanography knowledge of the density and current flow fields, together with conservative tracers, are the keys to understanding ocean dynamics. Unfortunately in paleoceanography the density (σ_t) field is elusive, though in special settings the relationship between benthic oxygen isotopic ratios and σ_t has been used [*Lynch-Stieglitz et al.*, 1999]. Also, most paleohydrographic tracers relate to nonconservative and/or biologically mediated properties. Thus a direct measure of flow speed would be very useful for inference of past ocean behavior, especially in conjunction with water mass tracer data. The flow speed we refer to is the geostrophic speed occurring above the Ekman layer or bottom mixed layer, 20–100 m above the bed.

[3] At the outset it must be remembered that at any given level in a core of fine sediment the last thing that happened to it of dynamical significance was that it was deposited. As *Dyer* [1986] so elegantly put it, "...there are large areas of the seabed where the sediments are cohesive until they move, and are noncohesive until they are deposited."

[4] Sedimentologists have long related particle size to the speed of the depositing or eroding flow. In the great majority of cases this has been for noncohesive sands and gravels via grain size and sedimentary structure analysis. Grain-size measurement of fine sediments prior to about 1970 was almost entirely by the pipette method [*Krumbein and Pettijohn*, 1938; *Galehouse*, 1971], and the results were used to define "texture" on sand-silt-clay triangular diagrams [e.g., *Folk*, 1954]. There were some attempts to relate fine size to dynamics, for example the coarsest 1% versus mean size plots of *Passega* [1957], but these did not go far beyond texture. The advent of the electrical resistance pulse counter (Coulter Counter) [*Sheldon and Parsons*, 1967], especially the 16-channel Model T in 1970, provided new high-resolution particle size data for sizes down to 0.5 μm at $^1/_3$ phi resolution. Early applications of this instrument and its cousin, the Elzone Counter, were to oceanic suspended sediment [*Brun-Cottan*, 1971], shallow marine sands [*McCave and Jarvis*, 1973] and deep-sea muds [*Ledbetter and Johnson*, 1976]. In particular it was the work of Ledbetter that led the way for use of fine particle size as a flow speed indicator. Subsequently other analytical methods were developed, laser diffraction sizers, X-ray scanning settling tube (SediGraph) and the Coulter Counter with up to 256 channels, all giving very high resolution data [*Singer et al.*, 1988; *McCave and Syvitski*, 1991; *Syvitski et al.*, 1991].

[5] Few attempts have been made to relate fine particle size to changes in current strength, the only one of significance being *Ledbetter* [1986a] (Figure 1). Traditional textural diagrams display gross aspects of sorting, but not in a way that can be used as an index of current strength. In sand-sized sediments the characteristics of stratification and bedforms (ripples, dunes, etc.) may be used to estimate paleocurrent strength, minimum flow speeds can be obtained from critical erosion curves, and modes of transport and shear stresses can be inferred from the shape of size distributions. Deep-sea currents are rarely able to move quartz sand [*Masson et al.*, 2004], but can in places move foraminiferal sand to form dunes [e.g., *Lonsdale and Malfait*, 1974], and appropriate critical movement curves have been developed for this material [*Miller et al.*, 1977; *Miller and Komar*, 1977]. Such occurrences involve sufficiently frequent movement of sand that the fine fraction is resuspended and carried away to leave a foraminiferal residue or lag, usually with low accumulation rates and lack of stratigraphic resolution. Periods of high current speed may therefore often be inferred from foraminiferal sands, but with the penalty of low temporal resolution and reworked foraminifera. Therefore, for paleocurrent reconstruction at high temporal resolution, sensitive parameters from rapidly accumulating and continuously deposited fine sediments are needed. As these normally show few structures other than biological disturbance, grain size parameters are required. It is important to remember that for fine sediments (but not for sands) the disaggregated state in which the samples are analyzed is not the state in which they were deposited, because that involved varying degrees of particle aggregation. Therefore dynamical inferences may not be made from the properties of the whole undifferentiated size distribution.

2. Theoretical and Experimental Basis

2.1. Arguments of *McCave et al.* [1995a]

[6] The basis for the "sortable silt" flow speed proxy was set out in some detail by *McCave et al.* [1995a], so the arguments given then are recapit-

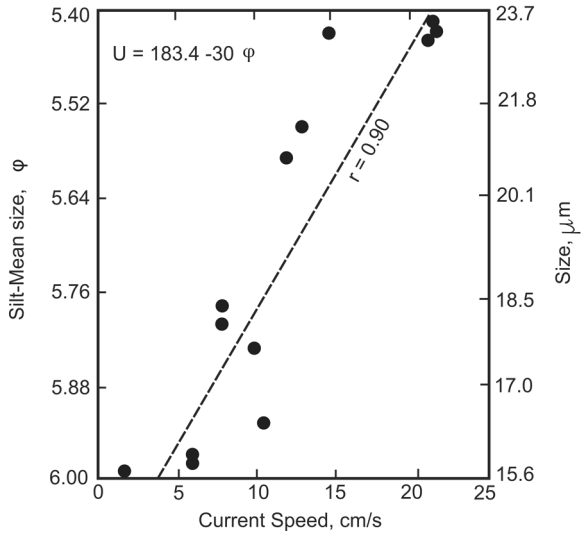

Figure 1. Calibration of "silt-mean size" to current meter data from Vema Channel by *Ledbetter* [1986a]. The size is the mean of the range of the Elzone instrument, 7.7- 4 φ (4.8–63 μm).

ulated only briefly here. The method proceeded from theory and observations in the High Energy Benthic Boundary Layer Experiment (HEBBLE) area on the Nova Scotian continental rise showing that the terrigenous (i.e., biogenic carbonate and silica removed) grain size distributions showed a pronounced mode in the part of the spectrum >10 μm in regions and at times when the flow speed was faster [*Hollister and McCave*, 1984; *Driscoll et al.*, 1985; *McCave*, 1985] (Figure 2). The terrigenous silt fraction was accordingly divided into two fractions, 2–10 μm cohesive silt dominated by clay minerals and 10–63 μm sortable silt (SS) of quartz and feldspar, with carbonate in both fractions. The mean size of the latter fraction (denoted by $\overline{SS}$) was proposed as a more sensitive indicator of the flow speed of the depositing current than the total "silt mean size" of *Ledbetter* [1986a] which included material from ~4–10 μm in a total range of 4–63 μm. The percentage of sortable silt (SS%) in the total <63 μm terrigenous fraction was also suggested as an index of current-controlled grain size selection.

[7] Many grain size analyses of sediments recovered from several contourite drifts made with different instruments show a minimum in the size distribution between about 8 and 10 μm. This was attributed to the tendency of material finer than about 8–10 μm to behave cohesively and coarser material to behave noncohesively and be current sorted by primary particle size (actually by settling velocity, w_s). The transition to cohesive particle behavior occurs partly because clay minerals, with their charge imbalances, enter the compositional spectrum [*Weaver*, 1989, p. 10]. Also, below this size, van der Waals forces become significant in particle adhesion [*Russel*, 1980]. For equal sized quartz grains at 50 nm separation, the ratio of forces due to van der Waals attraction and particle weight is 0.2 for 10 μm, and 20 for 1 μm diameter. The critical erosion behavior of quartz in seawater, shows that cohesion starts to dominate for sizes less than about 10 μm [*Unsold*, 1982] (Figure 3). These data are not so precise as to specify 10 μm exactly, and the region 8 μm (= 7 phi) to 11 μm (6.5 phi) was considered a transition region for this behavior, but for the sake of definiteness 10 μm was used. Below that size deposition is dominated by aggregates from which dynamical inferences can only be made on the basis of modeling with several assumptions (see *Curran et al.* [2004],

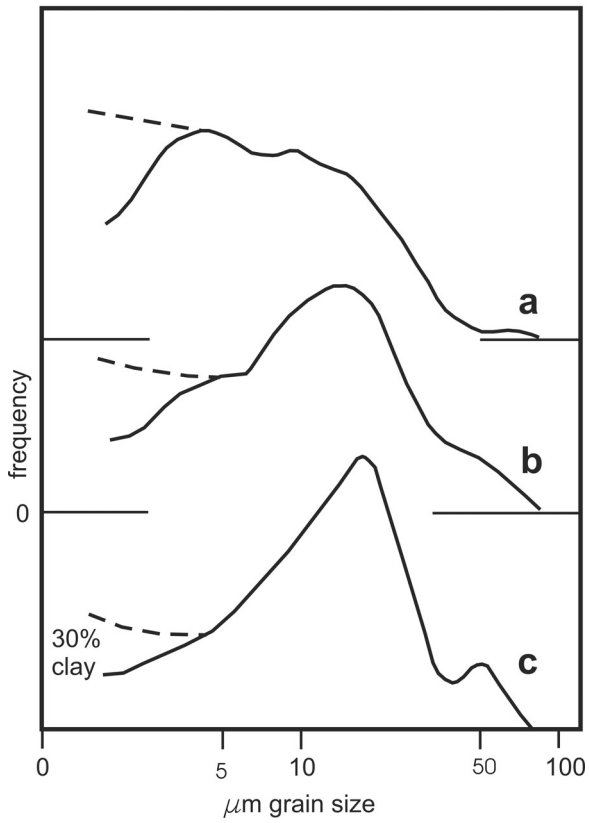

Figure 2. Size distributions of sediment from the Nova Scotian Rise measured by Coulter Counter (from *McCave et al.* [1995a]) showing deposits (a) under slow currents at 4000 m water depth, (b) after moderate currents of 5–10 cm s^{-1} at 4800 m, and (c) after strong currents (10–15 cm s^{-1}) at 4800 m.

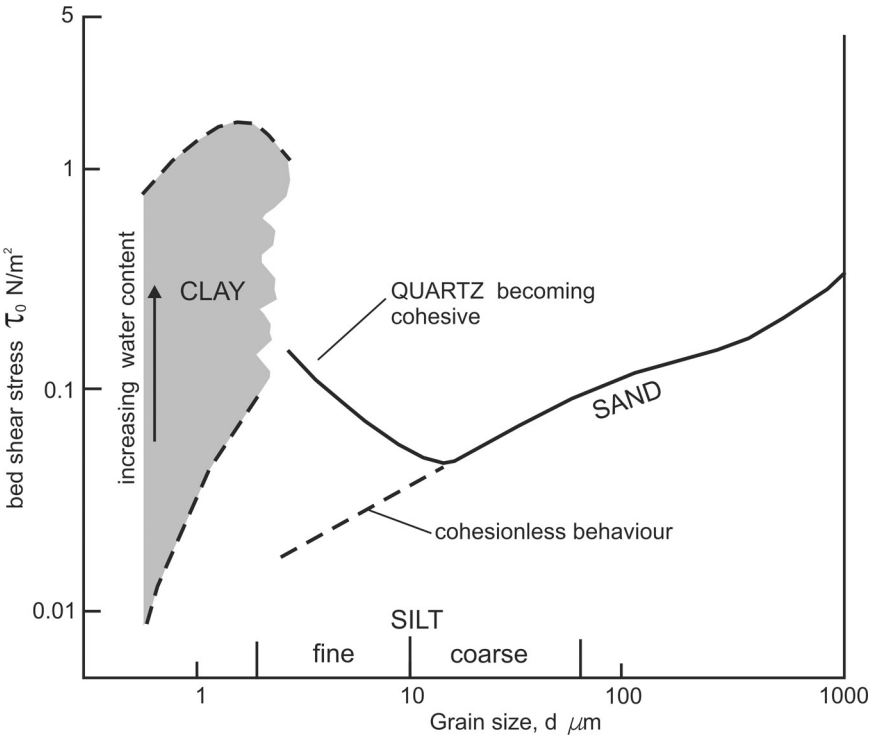

Figure 3. Critical erosion flow shear stress versus grain size showing noncohesive behavior down to about 10 μm and cohesive behavior below that with a strong dependence on water content. After *McCave et al.* [1995a].

discussed below). (Aggregates comprising several to many particles are also known as flocs, and the aggregation process as flocculation. There is a tendency in the literature to use "aggregate" when there is biological mediation in their production or cohesion, and "floc" when simply physical mechanisms and electrochemical attraction are involved, though there are many exceptions. Here we tend to use "aggregate" except where the cited author (especially Kranck) has used "floc." See *McCave* [1984], *Winterwerp and van Kesteren* [2004], and *Thomsen* [2005] for details.) The choice of this size region has recently received support from an unexpected quarter in the results of *Chang et al.* [2005] who shows a pronounced minimum in size frequency centered on 8.6 μm (6.85 phi) on muddy tidal flats.

[8] Sediment sorting occurs principally during resuspension and deposition by processes of aggregate breakup and particle selection according to settling velocity and fluid shear stress (τ). The controlling variables are critical erosion stress (τ_e), critical suspension stress (τ_s) and critical deposition stress (τ_d). In general $\tau_d < \tau_e < \tau_s$ for noncohesive material. During deposition some grains and aggregates are sorted by being trapped in the viscous sublayer of a turbulent boundary layer, while others of smaller settling velocity are not trapped, but kept in turbulent suspension and transported further downcurrent. Sorting of muds thus arises mainly from selective deposition. Selective erosion (winnowing) is a less important sorting process for cohesive muds as the cohesion means that removal of the particles which are most prone to stick together is not strongly size selective [*Winterwerp and van Kesteren*, 2004; *Schaaff et al.*, 2006]. It can make the deposit somewhat coarser overall by producing intermittent erosion horizons marked by coarse silt–sand lags, but at the cost of decreasing accumulation rate (see sections 2.3 and 2.4).

[9] The critical deposition stress (τ_d) is the stress below which particles of a given settling velocity will deposit, while those of smaller settling velocity will be ejected from the viscous sublayer. This stress according to *Self et al.* [1989] is $\tau_d \approx 10^3 d$ (in S.I. units), thus deposition of 10 μm particles occurs at stresses <0.010 Pa (shear velocity $u_* <$ 0.32 cm s^{-1}). These values, obtained in a radial laminar flow cell, are rather less than the critical deposition stresses from *McCave and Swift* [1976] which yield $\tau_d \sim 0.045$ Pa ($u_* = 0.67$ cm s^{-1}) for 10 μm silt, or via the analytical expression of *Dade et al.* [1992] giving 0.015 to 0.03 Pa. The trend of

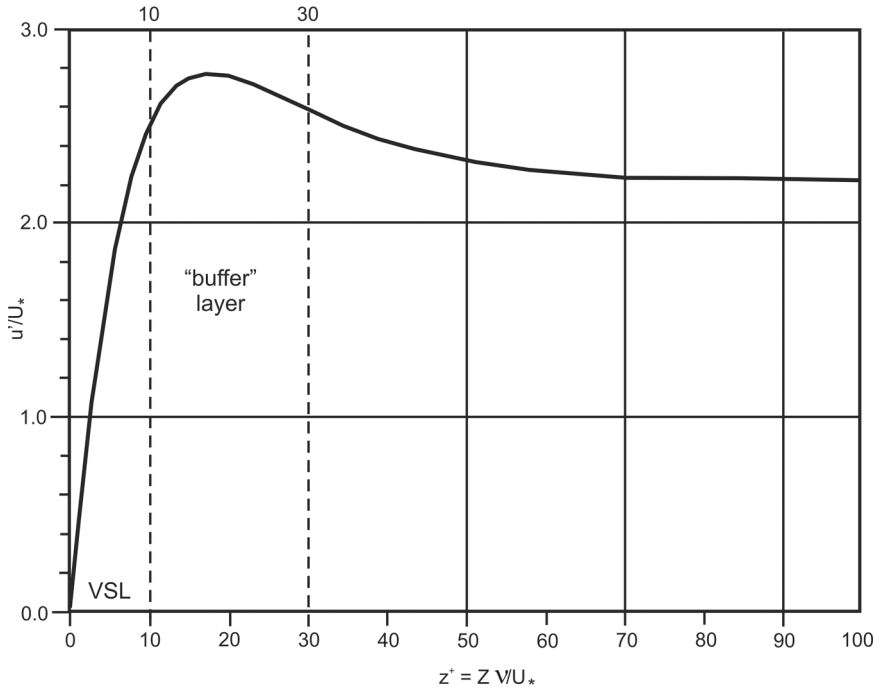

Figure 4. Turbulence intensity from *Nezu and Nakagawa* [1993], showing maximum turbulent intensity (ratio of RMS turbulent u' fluctuations to mean flow U speed) in the "buffer layer." The nondimensional distance above the bed z^+ of 10–30 is equivalent to 1 to 10 mm to 3 to 30 mm under conditions from slight erosion to rapid deposition. Under conditions relevant to the breakup process the stress maximum is closer than 5 cm to the bed.

these curves, however, is the same. This range of shear stresses (0.01–0.045 Pa) is a little lower than that indicated by *Hunt*'s [1986] experiments for the breakup of montmorillonite and illite flocs due to shear, namely 0.04 to 0.16 Pa (shear rates (Γ) of 4 to 16 s^{-1}). The implication is that most aggregates less than about 10 μm in diameter will survive during deposition from currents. However, above that size aggregates are increasingly likely to be broken up in the "buffer layer" located just above the viscous sublayer where large turbulent shear fluctuations occur (Figure 4). Hydrodynamic processes of sorting in the viscous sublayer will thus tend to act on primary particles for sizes greater than 10 μm. Consequently under stronger flow this material will be size-sorted according to its primary grain size allowing the use of the SS component as an index of the flow speed of the depositing current.

2.2. Sediment Deposition and Grain Size Distributions

[10] The basic equations governing the deposition of sediment from suspension are

$$C_t = C_o \exp -(K_t w_s); \qquad C_x = C_o \exp -(K_x w_s) \quad (1)$$

where for deposition as a function of time t, $K_t = (tp/h)$ and as a function of distance x, $K_x = (xp/hU)$, and p is the probability of deposition given by $p = (1 - \tau_o/\tau_d)$, in which the boundary shear stress τ_o is less than τ_d the limiting stress for deposition, h is thickness of the suspension and U is flow speed [*Sundborg*, 1956; *Einstein and Krone*, 1962].

[11] The work of *Kranck and Milligan* [1985, 1991] and *Kranck et al.* [1996a, 1996b] argued that the size distribution of fine sediment could be represented as due to a combination of floc and grain deposition. Deposition of flocs containing a wide range of mainly smaller particles produced a poorly sorted deposit and was favored by a high degree of flocculation, low transport energy and few or no resuspension events. The boundary between floc and grain-dominated deposition lay around 10 μm (Figure 5). *Kranck and Milligan* [1985] noted the similarity of their measured size distributions to the Rosin-Rammler distribution and proposed the fine end of the size spectrum to have the related form

$$dV/d(\log d) = C_o w_s^m/\beta \quad (2)$$

where C_o is the concentration at a nominal size (e.g., $d_o = 1$ μm), β is the coefficient in Stokes law

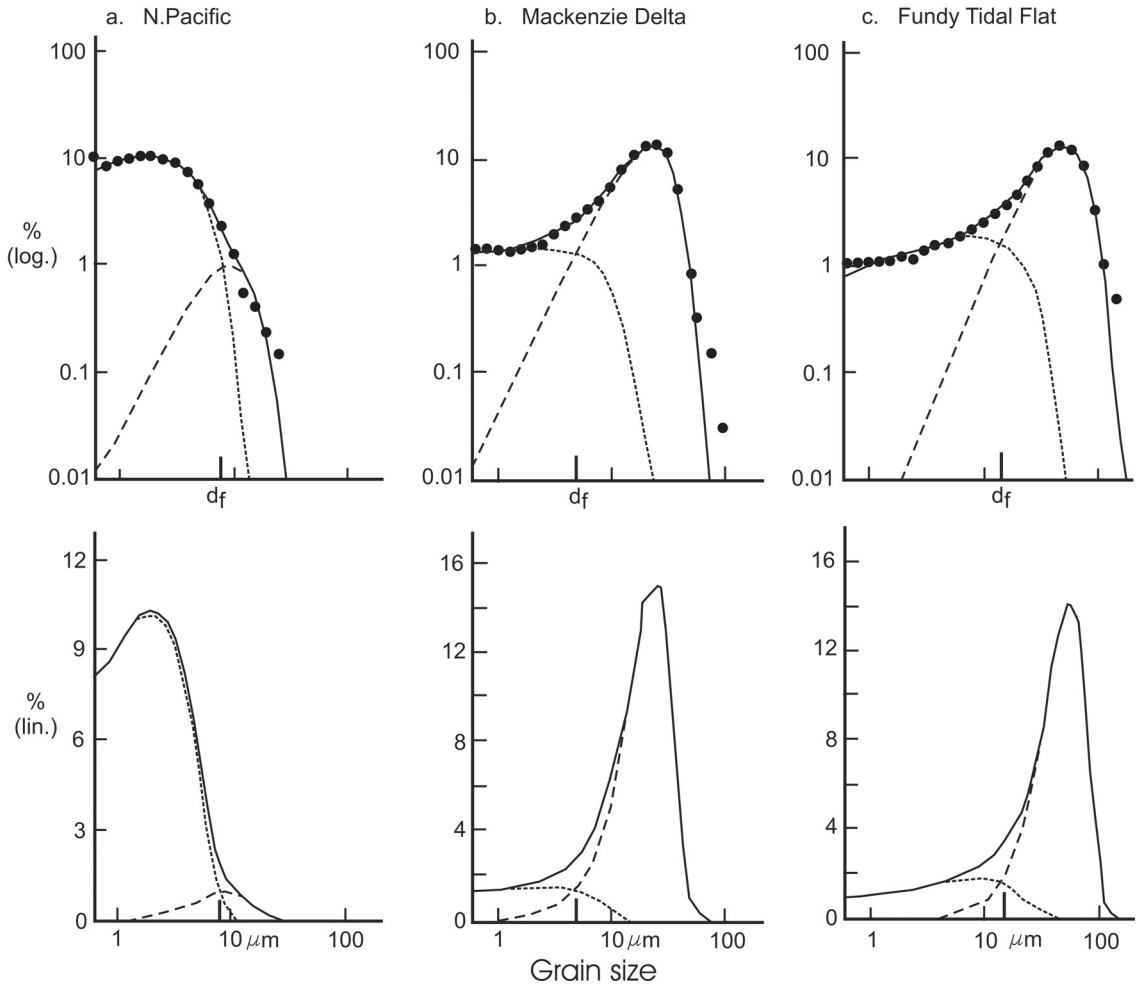

Figure 5. Three grain size spectra from *Kranck and Milligan* [1991] partitioned into floc-deposited (dotted lines) and grain-deposited (dashed lines) components. Top row log-log plots; lower row same data as log linear plots. Data from Coulter counter analyses. The "floc limit" (d_f), size of equal floc and grain contribution to the distribution, ranges around 10 μm. Flow energy of depositional setting increases left to right, deep to shallow.

relating settling velocity to diameter ($w_s = \beta d^2$), and m is the slope of the distribution, generally in the region 0 ± 0.2, i.e., fairly flat (an unsorted distribution containing equal volumes of particles in logarithmically increasing size grades has $m = 0$, equivalent to a cumulative particle number distribution with a slope of -3, the Junge distribution of aerosol literature). *Kranck and Milligan* [1991] represented the size distribution of a depositing sediment suspension in the related form

$$C_i = C_o d_i^m \exp -\left(K_t \beta d_i^2\right) \quad (3)$$

based on deposition rates of fractions (i) being proportional to the exponential of their settling velocity or d^2. Their version of the parameter K_t omitted p, the probability of deposition term in equation (1) above. However, p is important because it permits sorting through suppression of deposition of slower settling particles under faster flows with higher values of τ_o. (C_i is the concentration of grains of diameter d_i). The material carried in suspension has a distribution of concentration C_z as a function of height z given by the standard Rouse equation which, close to the bed, is $C_z/C_a = \exp(-\mathrm{Aw_s})$. In this the "reference concentration" C_a is specified at a height a and $A = \ln(z/a)/\kappa u_*$ with von Karman's constant $\kappa = 0.41$, and $u_* = (\tau_o/\rho)^{1/2}$ where ρ is the fluid density. If flow conditions change (e.g., a decrease in u_*, then K_t changes to K'_t), sediment is deposited and the size distribution of the deposit is

$$\mathrm{d}V/\mathrm{d}\left(\log d_p\right) = C_o \beta w_s^m \left[\exp(-K_t w_s) - \exp\left(-K'_t w_s\right)\right] \quad (4)$$

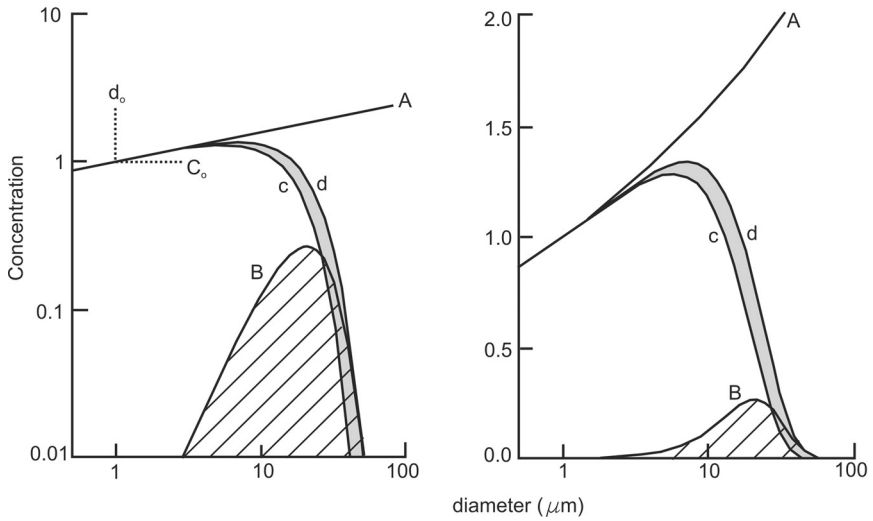

Figure 6. Diagrams showing the grain size distribution of a deposit from suspension where A is the original unsorted suspension (slope of this parent distribution is m = 0.2) and d and c are the distributions before and after a small reduction in concentration, resulting in deposit size distribution B (left, log-log; right, log linear). From *Kranck et al.* [1996a].

This is illustrated in Figure 6 where it is seen that a small change in K_t via a reduction in flow speed, permits a little of the coarse tail of the suspension to be deposited while the remainder continues in suspension transport. Repeated sorting events of resuspension, transport and fractional deposition would give a well sorted (small standard deviation) lognormal distribution according to *Middleton*'s [1970] arguments for sands.

2.3. Particle Aggregates, Breakup, and Sorting by Selective Deposition

[12] Fine sediment distributions may have a moderately well sorted silt mode but be overall poorly sorted. The fact that fine sediment distributions do not become well sorted is due to the effect of flocculation, often aided by organic means (see *Winterwerp and van Kesteren* [2004] for a recent review). This effect causes smaller particles in flocs to be deposited with larger individual grains where floc and grain settling velocities are similar. Nevertheless, fine sediments display sorting on the basis of size and mineralogy [*Gibbs*, 1977; *Mehta and Lott*, 1987]. *Mehta and Lott* [1987] argued for selective deposition on the basis of a presumed relationship between the critical deposition stress and settling velocity, and the likelihood of aggregate breakup close to the bed. Flocs are fragile [*Hunt*, 1986] and their presumed breakup near the bed in the buffer layer (Figure 4) appears to be borne out by some recent measurements in shallow water where particle size in suspension *decreases* toward the bed in the bottom ~1.0 m of the flow (Figure 7) [*Fugate and Friedrichs*, 2003]. This is still far above the buffer layer, but is much closer to the bed than the regions of flow in which large flocs are usually measured [*Dyer et al.*, 1996]. It has been argued that the floc size in the buffer layer is proportional to the Kolmogorov microscale $\lambda_k = (\nu/\Gamma)^{1/2}$ where ν is the kinematic viscosity and Γ is the shear rate $(\varepsilon/\nu)^{1/2}$ in which ε is the turbulent kinetic energy dissipation rate. If Γ is 100 s^{-1} (equivalent to $\tau_o = 0.1$ Pa) and ν is 10^{-6} m^2 s^{-1}, λ_k is 100 μm. However, that is the mean value. In the region close to the bed the *maximum* stresses are up to 8 times the mean, and the data of *Fugate and Friedrichs* [2003] suggests the median size is about half λ_k. These particles, conditioned by high near bed turbulence are deposited, whereas larger flocs formed higher up in the flow are transported. Sorting thus occurs by selective deposition of particles selected on the basis of settling velocity. Under relatively quiescent conditions of little floc breakage, fine size distributions are dominated by floc-deposited sediment (Figure 5a), whereas under more energetic conditions, deposition of the finer material is relatively suppressed (Figures 5b and 5c) and some sorting by active removal of fines, winnowing, may also occur.

2.4. Transport, Sorting in Deep-Sea Storms, and Deposition

[13] A large body of evidence has demonstrated the importance of deep western boundary currents

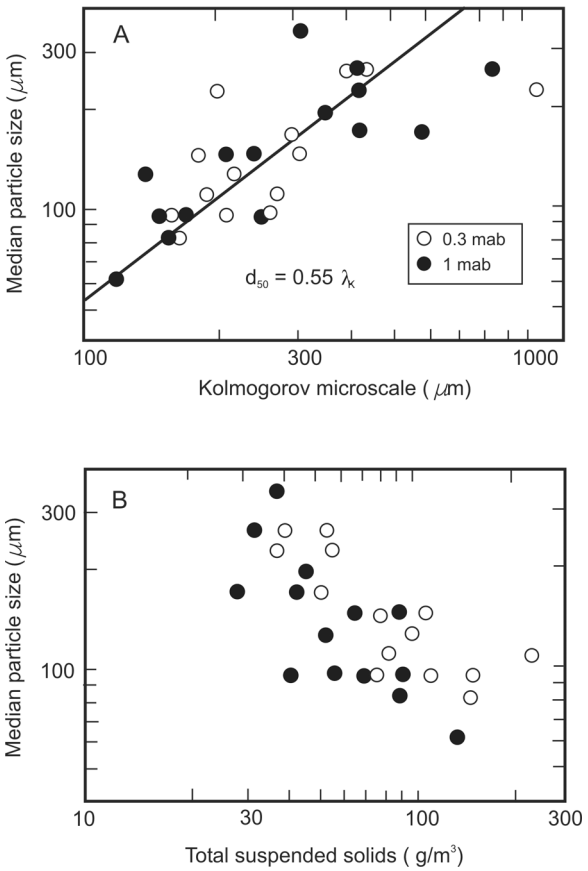

Figure 7. (a) Data from a laser in situ sizer (LISST) within 1 m of the bed (1 mab) showing a dependence of particle aggregate size on Kolmogorov microscale (λ_k) which decreases as shear increases closer to the bed. (b) Particle size decreasing with increasing concentration suggesting shear-induced breakup (whereas increasing size would be expected as collisions are more frequent at higher concentration). From *Fugate and Friedrichs* [2003].

(DWBC) to sediment transport and the deposition of especially thick sediment sections in contourite drifts [see, e.g., *Stow et al.*, 2002]. Typical sedimentation rates on drifts are 5–20 cm kyr^{-1}, exceptionally and locally over 100 cm kyr^{-1}. If one takes the global river sediment supply, removes 90% for deposition in deltas, nearshore and on slopes, and distributes the rest over the world ocean the rate is ~0.45 g m^{-2} yr^{-1}. Even allowing for a Pacific effect (ringed by trench sediment traps), the rate is still <1 g m^{-2} yr^{-1}, or <~0.125 cm kyr^{-1}. Even allowing for the facts that sediment is introduced to continental margins and that the ratio of margin to total ocean is 26% for the Atlantic and 15% for the Indian Ocean [*Menard and Smith*, 1966], it still means that rates over 0.5–1 cm kyr^{-1} represent focusing. Clearly high sediment focusing occurs in drifts. Carbonate sedimentation rates at 3760 m water depth under the eastern equatorial Pacific productivity maximum are <2 cm kyr^{-1} for the last 4 Myr (ODP Sites 851/1225), thus rates in excess of this are most likely also to involve current-driven focusing. The finer (nannofossil and diatom) components are focused as the foraminifera are rarely moved. Material has to be advected to the deposition site, usually from a region of higher velocity flow upstream, e.g., the flow of Iceland Scotland Overflow Water over the S. Iceland Rise turbidites upstream of Gardar Drift [*Bianchi and McCave*, 2000]. In such a drift setting this means that, with increasing current speed, there must first be an increase in accumulation rate followed by a decrease as intermittent erosion events start to dominate (Figure 8). At flow speeds below the peak accumulation rate the sorting will be dominated by selective deposition, whereas above that some winnowing also participates. Eventually, above some relatively high value of flow speed (about 20–25 cm s^{-1} is critical for movement of foraminifera [*Miller and Komar*, 1977]) conditions of net fines removal, i.e., winnowing, leaving a sandy residue, set in.

[14] The effect of zones of high current speed can be seen in the spatial distribution of grain size in ocean basins. This has been best shown by *Ledbetter* [1986b] in the Argentine Basin where there is a zone of higher silt mean size under the path of the northward flowing DWBC. A similar zone of higher size is shown under the Western Boundary Undercurrent (WBUC) on the US margin [*Bulfinch et al.*, 1982; *Bulfinch and Ledbetter*, 1984], and also on the Nova Scotian Rise by *Driscoll et al.* [1985] and, with photographs, *Tucholke et al.* [1985]. The zones of coarser size are also zones of more intense resuspension shown by locally higher turbidity along western boundaries of the Atlantic [*Eittreim et al.*, 1976].

[15] *Middleton* [1970] shows how repeated sorting events comprising suspension of sand on a beach, followed by redeposition of some of it and removal of part to the offshore, results in generation of a lognormal size distribution. The size sorting is actually controlled by the settling velocity of the particles determining whether they enter the deposit or move offshore. The deep-sea setting provides an analogous situation because of the unsteadiness of deep-sea currents resulting in so-called "deep-sea storms," periodic resuspension-

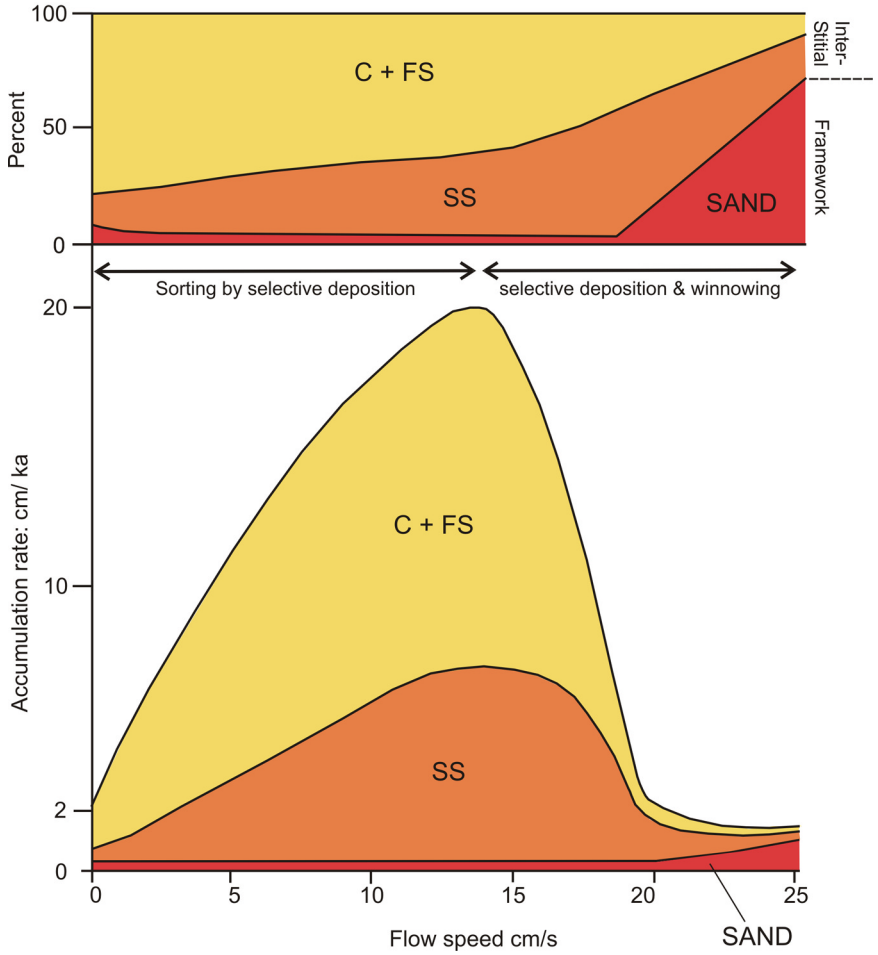

Figure 8. Hypothetical variation of accumulation rate with increasing current speed. C+FS, clay and fine silt (<10 μm); SS, sortable silt (10–63 μm). The "sand" here is a size term referring to both terrigenous and carbonate, mainly foraminifera, components. At zero speed a pelagic rate of 2 cm kyr^{-1} is assumed. From zero to the peak accumulation rate the sorting process is all selective deposition, whereas above that point, here arbitrarily put at a flow speed of 13 cm s^{-1}, it is a combination of selective deposition and removal of fines (winnowing). Erosional winnowing and some sand movement are assumed to occur above 20 cm s^{-1}. (That this is not always so is shown by Figure 1, where a silt calibration point is at 23 cm s^{-1}.) Above 20 cm s^{-1}, mud will be mainly interstitial in sand, while above ~30 cm s^{-1} (not shown) the sand will be sufficiently mobile to contain little mud at all and will be forming ripples and sand waves. The curve is shown as peaking between 10 and 15 cm s^{-1}, but this is not at all well zknown and may well be dependent on the magnitude-frequency structure of deposition and erosion events. A peak around 10 cm s^{-1} would be entirely feasible as some records suggest the onset of surface erosion above 10–12 cm s^{-1} [*Gross and Williams*, 1991].

transport-deposition events [*Hollister and McCave*, 1984; *Gross and Nowell*, 1990; *Gross and Williams*, 1991; *Richardson et al.*, 1993] As seen in (Figure 9) the response of the suspended sediment concentration field to forcing is complex with evidence of (A) local erosional supply, (B) advection of turbid pulses eroded elsewhere, (C) supply limitation, possibly controlled by the surface reservoir of biologically conditioned suspendable material running out, (D) concentration decrease due to dilution in a thickening boundary layer, and (E) substantial periods of time with flow speed below 10 cm s^{-1} during which deposition occurred [*Gross and Williams*, 1991; *Gross and Nowell*, 1990]. In the Argentine Basin, good correlation was found by *Richardson et al.* [1993] between abyssal eddy kinetic energy and variations in suspended sediment concentration indicating local control. These regions of deep storms were linked by *Hollister and McCave* [1984] to regions of high abyssal eddy kinetic energy, particularly in western ocean basins and the Antarctic Circumpolar Current.

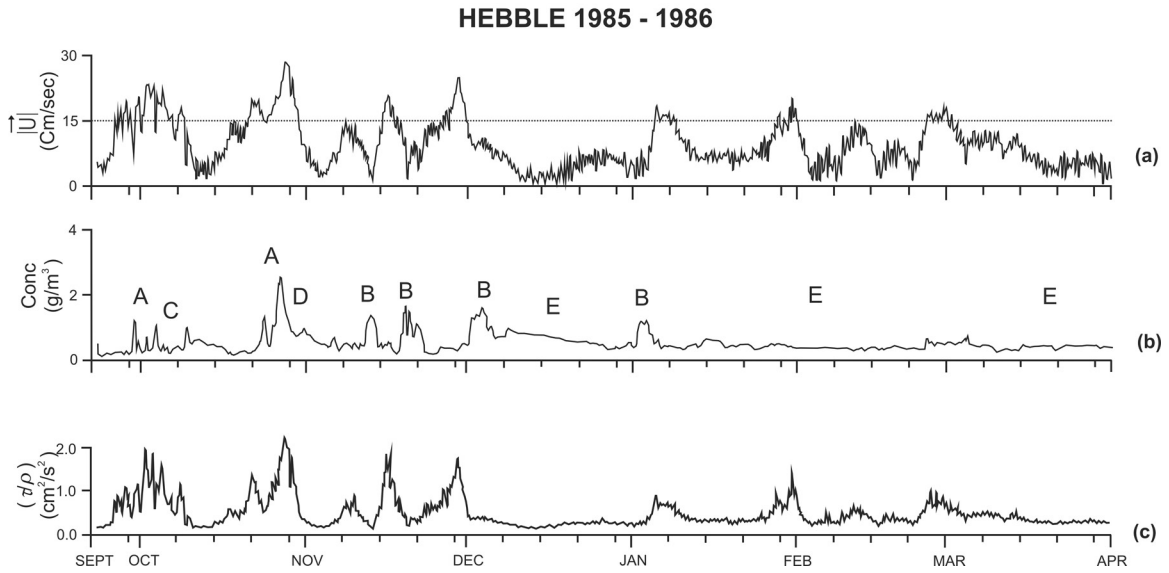

Figure 9. Benthic storms shown in part of the 1985–86 HEBBLE record of (a) flow speed, (b) turbidity (optical, converted to g m^{-3}), and (c) shear stress (as $\tau_o/\rho = u_*^2$) in the bottom boundary layer (speed at 4.9 meters above bottom (mab), turbidity at 2.2 mab) on the Nova Scotian Rise (4830 m water depth) [*Gross and Williams*, 1991]. The response of the suspended sediment concentration field to forcing is complex with evidence of events due to (A) local erosional supply, (B) advection of turbid pulses created by erosion elsewhere, (C) supply limitation, possibly controlled by the surface reservoir of biologically conditioned suspendable material running out, (D) concentration decrease due to dilution in a thickening boundary layer, and (E) depositional periods with flow speed below 10 cm s^{-1}. Lines have been put on the speed at 15 cm s^{-1}, about critical erosion conditions. (A value of $\tau_o/\rho = 0.5$ cm^2 s^{-2} is equivalent to $u_* = 0.71$ cm s^{-1} and $U_g \approx 13$ cm s^{-1}.)

Evidence of strong eddy activity has been found on most sediment drifts by current and/or turbidity records. Indeed it is an essential feature of the transport-deposition system because of the profound asymmetry of erosion and deposition (a few minute's erosion can remove several week's deposition). Putting the material into suspension takes a short time in storms and the intervening period is then occupied by sorting through selective deposition.

2.5. Covariance of $\overline{SS}$ and SS%

[16] In several cases a clear relationship can be seen between $\overline{SS}$ and SS% in the expected sense of the two increasing together (Figure 10a). In the case shown the dynamical range of $\overline{SS}$ is not great, from about 11.5 to 16.1 μm, but the increase of SS% with mean size indicates a sorting process that operates down to low SS percentages, about 4%. In another example, a wider range of $\overline{SS}$ (11.5 to 21 μm) is seen in a relatively narrow range of SS%, 2–10% (Figure 10b). There are also some very high values of SS%, up to 50%, generally associated with high values of the mean size. This suggests that (1) there is a wide dynamical range of the $\overline{SS}$ at fairly low percentages of SS, extending to well below 5%, and (2) the $\overline{SS}$ proxy is not compromised in cases of supply limitation of the coarse silt fraction to <10% in the SS fraction (Figure 10b). As will be discussed below, the data set shown in Figure 10b gives a reliable power spectrum and cross-spectrum coherent with benthic $\delta^{18}O$, and the range of values at low SS% is not dominated by error [*Hall et al.*, 2001; *Bianchi et al.*, 1999].

3. Measurement of Fine Grain Sizes

3.1. Particle Size Analysis Instruments and Methods: Pitfalls and Limitations

[17] This topic is covered at length in several recent publications and is only briefly summarized here. Several types of instrument, based on fundamentally different theoretical underpinnings, are available for the measurement of grain size distributions. Each analytical device has its disadvantages and one instrument may be better suited for a specific application rather than another [*McCave and Syvitski*, 1991]. None of them actually mea-

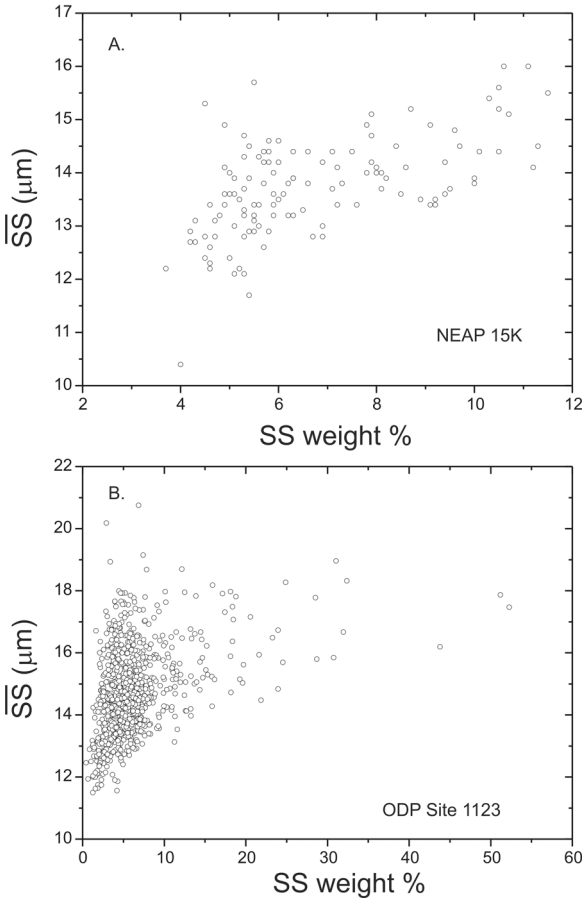

Figure 10. (a) Plot of $\overline{SS}$ versus SS% for the Holocene section in NEAP 15K [*Bianchi and McCave*, 1999] showing clear relationship (r = 0.59). The $\overline{SS}$ intercept of a reduced major axis at 0% is 10.6 μm. (b) Similar plot for 0–1.2 Ma of ODP Site 1123 [*Hall et al.*, 2001] showing clear relationship, but greater scatter with some high SS% values.

sures size. Presently, the Sedigraph is the instrument of choice for the study of deep-sea sediments as proxies for current intensity, since it is based on the settling velocity principle and therefore measures a "dynamical" grain size distribution closely related to transport and depositional processes. *Bianchi et al.* [1999] illustrated how the Coulter Counter, measuring a volume-equivalent spherical diameter inferred from electrical conductivity, constitutes a viable alternative to the Sedigraph, especially when the relative abundance of material in the SS range does not exceed 5%. Broadly, methods of size measurement may be divided into those which yield information on the whole size distribution, and those for which the information comes from a size window with upper and lower limits. A Coulter Counter performs an analysis with a detection window of ~2–50% of the diameter of the orifice through which the particles are sucked and sensed. Commonly 100 or 200 μm apertures are used giving sensed ranges of 2 to 50 μm and 4 to 100 μm. The Coulter Counter does not record the <2 μm clay that may comprise a significant part of the size spectrum, unless a very small aperture is used (which is difficult to operate and still has a lower limit of 0.5 μm) [*Milligan and Kranck*, 1991]. This means that the Coulter Counter can record only $\overline{SS}$, not SS%, the percentage of the <63 μm fraction that is 10–63 μm.

[18] Laser particle sizers should be avoided for paleocurrent reconstructions because the measured size of platey minerals can be dominated by their large projected area [*Konert and Vandenberghe*, 1997; *McCave et al.*, 2006]. This causes them to be recorded as the same size as larger equant grains although they have much smaller settling velocity and were deposited in aggregates. This yields results with a weaker relationship to the dynamics of deposition. The central problem is that some coarse clay/fine silt is recorded as medium to coarse silt, the key size in the sortable silt mean size method of inferring changes in flow speed. The performance of a laser sizer was compared with results from a Coulter Counter by *McCave et al.* [2006]. It is clear from their results that there are important instrumental differences associated with the determination of the fine silt-clay fraction in deep-sea sediments by laser sizers which limit their application in determination of paleocurrent sensitive parameters, in particular the $\overline{SS}$ paleocurrent speed proxy. While this has not been checked on instruments other than the Malvern MultisizerX and 2600E, it is probably true of all that employ the principle of inverting the angular distribution of forward-scattered light intensity to yield the most probable grain size distribution, when they encounter platey particles. It is not just that the data are not comparable with the Coulter Counter and Sedigraph, it is that particle shape-related artifacts occur at the crucial part of the size spectrum on which paleocurrent inference depends (10–~25 μm). These artifacts are not always present, a variability that is all the more damaging for comparative purposes. Laser sizers are excellent for sizing of equant grains, coarse silt and sand. They have given accurate results for aeolian loess (coarse to very coarse silt) where SS% is generally >40% [e.g., *Ding et al.*, 2002], and provide the only wide spectrum (1–1000 μm) method of analysis.

[19] In summary: measurements using a sedimentation principle (e.g., pipette method, Sedigraph) are capable of sensing the total amount of material present and giving a fairly accurate measurement of the 1 to 70 μm size distribution (but beware of montmorillonite [*Stein*, 1985]) [*Coakley and Syvitiski*, 1991]. Electrical sensing zone counters (Coulter, Elzone) give an accurate measurement in the 0.5 to 100 μm range, but do not see anything outside the detection window of the chosen sensing aperture; in particular, they miss some of the clay. Laser diffraction sizers (Malvern, CILAS, Horiba, Fritsch, Coulter, Sympatek) also give a fairly accurate representation of the size distribution for material over about 30 μm, but in the lower SS range (10–30 μm) suffer from the effect of the platey shape of clay and fine silt particles which results in them being seen as the same size as coarser equant grains and contaminating the size distribution up to about 30 μm [*Agrawal et al.*, 1991; *Konert and Vandenberghe*, 1997; *Xu*, 2000; *McCave et al.*, 2006]. Comparisons of several instruments are given by *Stein* [1985], *Singer et al.* [1988], *Syvitski et al.* [1991], *Weber et al.* [1991], *Bianchi et al.* [1999], and *McCave et al.* [2006].

3.2. Size of Components by Removal, Repeat Analysis, Scaling, and Subtraction

[20] The size distribution of compositionally distinct parts of the sediment can be obtained by determining the size distribution of the sediment before and after removal of the component and determination of its amount. The most obvious one is carbonate. The total fine fraction is size analyzed, carbonate is removed, and the proportion of carbonate, C (where $1 > C > 0$), is determined on a subsample. The size distribution of the residue is then determined. The size distribution of the carbonate is given by the difference between the size distribution of the total minus $(1 - C)$ times the size distribution of the residue. Formally, in unit mass of sediment, defining the size distribution function $f(d_p)$ as $f(d_p) = dm/dd_p$ where dm is the mass of particles between size d_p and $(d_p + dd_p)$, then

$$f(d_p)_C = f(d_p)_T - (1 - C) f(d_p)_R$$

where the subscripts C, T and R denote the carbonate fraction, total sediment and noncarbonate residue, $T = (C + R) = 1$ [*McCave et al.*, 1995a]. When the sediment also contains a significant amount of biosiliceous debris (diatoms, radiolarians), further removal steps are necessary, rendering the whole procedure very involved. This technique was originally used by *Paull et al.* [1988] and *Wang and McCave* [1990]. More recently, *Trentesaux et al.* [2001] and *Frenz et al.* [2005] have inferred carbonate grain-size distributions and foraminifer and coccolith size components in hemipelagic sediments.

[21] The $\overline{SS}$ parameter for inference of flow speed is mainly based on use of the terrigenous fraction because biogenic material often carries specific size modes characteristic of the species involved. This material can in cases also be sorted. *Wang and McCave* [1990] show an example where the carbonate size spectrum parallels the terrigenous component size between glacial and interglacial flow conditions. However, it has been found that in most cases the biogenic component simply confuses the signal by adding noise or a species-related size, so it is generally removed without the double sizing procedure described above.

4. Problems

4.1. Critical Deposition Conditions

[22] The critical erosion curve over the 12–30 μm region is rather flat, particularly if expressed in flow speed ($\propto$ square root of the stress shown in Figure 3). The variation in shear stress implies an increase of only 20% in flow speed over this range, so how can there be a strong sorting effect? A similar flat curve is predicted by *Self et al.* [1989]. The calibration of *Ledbetter* [1986a] (Figure 1), however, suggests much greater sensitivity of silt size to flow speed. Following the arguments of *Kranck and Milligan* [1985, 1991] given above we suspect that it is the relationship with particle settling velocity that controls rate of deposition and is proportional to d^2. It is the objective of work in progress to relate SS to flow speeds recorded by deep-sea long-term current meters (see below).

4.2. Particle Source Changes

[23] It is commonly, but erroneously, presumed that source exerts a dominant influence on size. For fine sediments source effect is far less of a problem than it is for sands, where, for example, there can be a strong influence of source rock on size, and size on mineralogy. Work on particle sizes of fine suspended sediment record a wide range. It is poorly sorted both at fluvial source [*Gibbs*, 1967; *Potter et al.*, 1975; *Johnson and Kelley*, 1984] (Figure 11) and in the sea [*Brun-Cottan*, 1971;

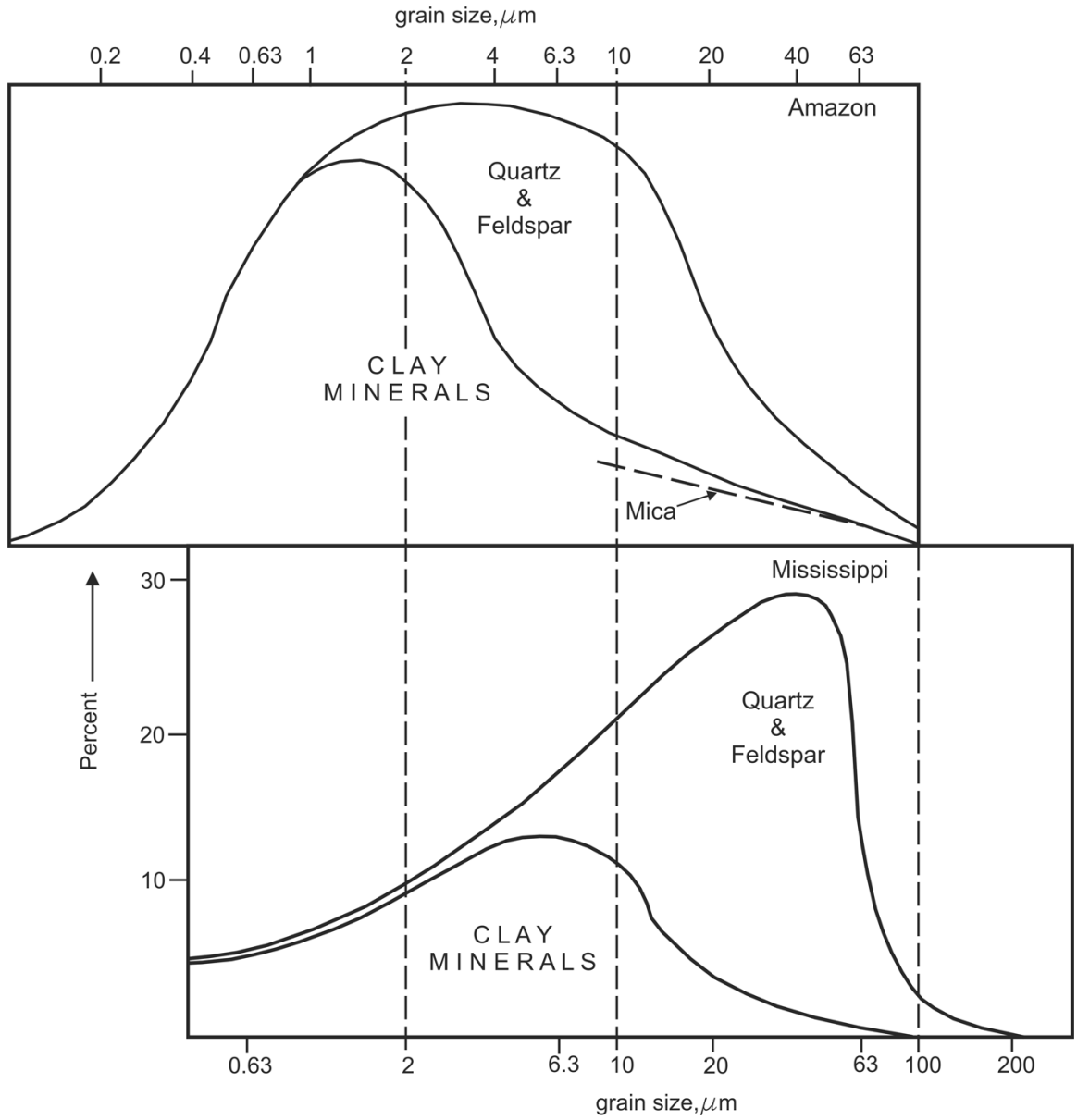

Figure 11. Size distribution of clay mineral and other components of river sediment from the Amazon [after *Gibbs*, 1967] and the Mississippi [after *Potter et al.*, 1975], showing that clay minerals of platey shape extend well above the clay mineral size of 2 μm used for X-ray diffraction analysis. The clay in the Mississippi coarse silt range is dominantly mica, but below $\sim$10 μm this is illite. (From *McCave et al.* [2006]).

McCave, 1983; *Kranck and Milligan*, 1983]. The size distribution dV/d(log d) versus log d is typically fairly flat (slope of zero $\pm$ 0.2), equivalent to a cumulative particle number distribution with a slope of -3 (the "Junge distribution" of aerosol literature). Mixing of several meters to tens of meters thickness of failed seabed in gravity flows delivering sediment to the deep sea (turbidity currents, debris flows) results in elimination of effects due to systematic temporal variability of sources on at least short timescales (order of at least 100 kyr, maybe to 1 Myr) [*Embley and Jacobi*, 1977; *Weaver and Thomson*, 1993]. Only in cases where sediment with a distinct sorted size spectrum is delivered to a relatively quiescent deep e.g., loess, beach sand, aeolian dunes spilling over low-stand shelf edges, will there be a strong source signature in the deposit. This is shown by *Holz et al.* [2004], who show, through dissection of the size distributions of slope sediments off NW Africa, that a recognizable aeolian dust signature is present. Clearly there are some sources that do

not produce gravel or coarse sand, but few that supply something fail to provide mud (clay plus some silt) as this comprises well over 50% of all sediment on Earth.

4.3. Problems of Cryptic Downslope Supply

[24] One insidious way in which size distributions can be influenced by processes other than bottom currents and record a source-related signature is by the fine tails of turbidity currents. Major turbidity currents with coarse bases and grading, and debris flows, are fairly obvious. They can generally be recognized by a combination of visual/X-radiographic observation, magnetic susceptibility and reflectance spectrometry, and be eliminated from the analyzed section as representing negligible time. The potential influence of the fine tails of turbidity currents entrained in deep current systems on continental margins is more subversive because it is largely unrecognized. It might be recognizable through periodic variability in some physical properties or the assemblage/abundance of microfossils, but as the frequency is likely to be in the centennial band most workers will latch onto these as evidence of climatic variation. Sharp bases will not be seen because of bioturbation. *Hall and McCave* [2000] called on this process to explain some anomalously coarse sizes on the Iberian margin at the Last Glacial Maximum (LGM). They found another nearby record (though from further upslope and possibly not in the same water mass) which did not show the anomaly but demonstrated reduced LGM flow, as expected from all the other cold periods in the record. However, there was nothing in the physical properties or X-radiographs to alert us to this problem. It remains one of the problems of continental margin sites.

[25] A particular site on the California continental slope under the California Current, ODP Site 1017 at 955 m depth, shows variation in the sortable silt range probably related to off-shelf downslope transport [*Behl et al.*, 2000]. The margin is also influenced by the poleward-flowing California Undercurrent which presently does not extend to the bed at Site 1017, though it is possible that these currents may have influenced sediment transport here in the past. *Behl et al.* [2000] argue that if grain size on the slope were primarily controlled by current action (i.e., coarser intervals are contourites), then mean grain size and sediment sorting would be positively correlated, both increasing with current strength (increased ("better") sorting = reduced standard deviation). This is not the case in their data as grain size is negatively correlated with sorting, and resolution of the size spectra into components also shows that increased abundance of the coarse silt component results in poorer sorting: more coarse material is not associated with less clay. Also symptomatic of downslope transport is the fact that the coarsest mode extends from 39 μm up into the fine sand range. A little caution is required as these results were partly generated by laser sizer which tends to enhance medium silt abundance, but not fine sand (see section 3.1). Sea level control is reflected in increased grain size related to enhanced resuspension and transportation off the shelf, during lower sea levels. Sea level control is also suggested by the observation that the finest mean grain size and best sorting occur at the time of highest sea level, $\sim$130–120 ka.

4.4. Local Spatial Variability of Flows and Particle Sizes

[26] Flow near the bed is strongly controlled by local topography and this is reflected in sediments. One well documented case is the variation over mudwaves [*Ledbetter*, 1993; *Manley and Flood*, 1993]. Mudwaves can behave either like dunes migrating in the direction of flow, or, perhaps more commonly, like antidunes responding to in-phase lee waves in the stratified water column. In the latter case the flow slows down on the upstream face yielding maximum deposition rate and speeds up over the downstream face resulting in slower deposition or erosion and coarser silt. This is expressed in the theories of *Flood* [1988] and *Blumsack and Weatherly* [1989], and, for the lee wave case, is corroborated by the grain size work of *Ledbetter* [1993]. Flow is also topographically steered by large sediment ridges. This results in the flow on one side being stronger than on the other due to Coriolis effects. The two sides of Gardar Drift [*Bianchi and McCave*, 2000] show clearly the reduced sedimentation rate and increased particle size on the eastern slope of the drift (Figure 12a) where Coriolis steepens the isopycnals driving a locally faster flow. This results in coarser sediments on the eastern side of the drift (Figure 12b).

[27] This gives potential for aliasing of inferred flow speeds downcore. This is not very likely for movement of drifts which are too large to move much even on a 1 Myr scale. But mudwave migration on the 100 kyr timescale could result in the stoss and lee sides of waves being sampled successively downcore, with size variations giving the impression of a time-varying flow, even if flow

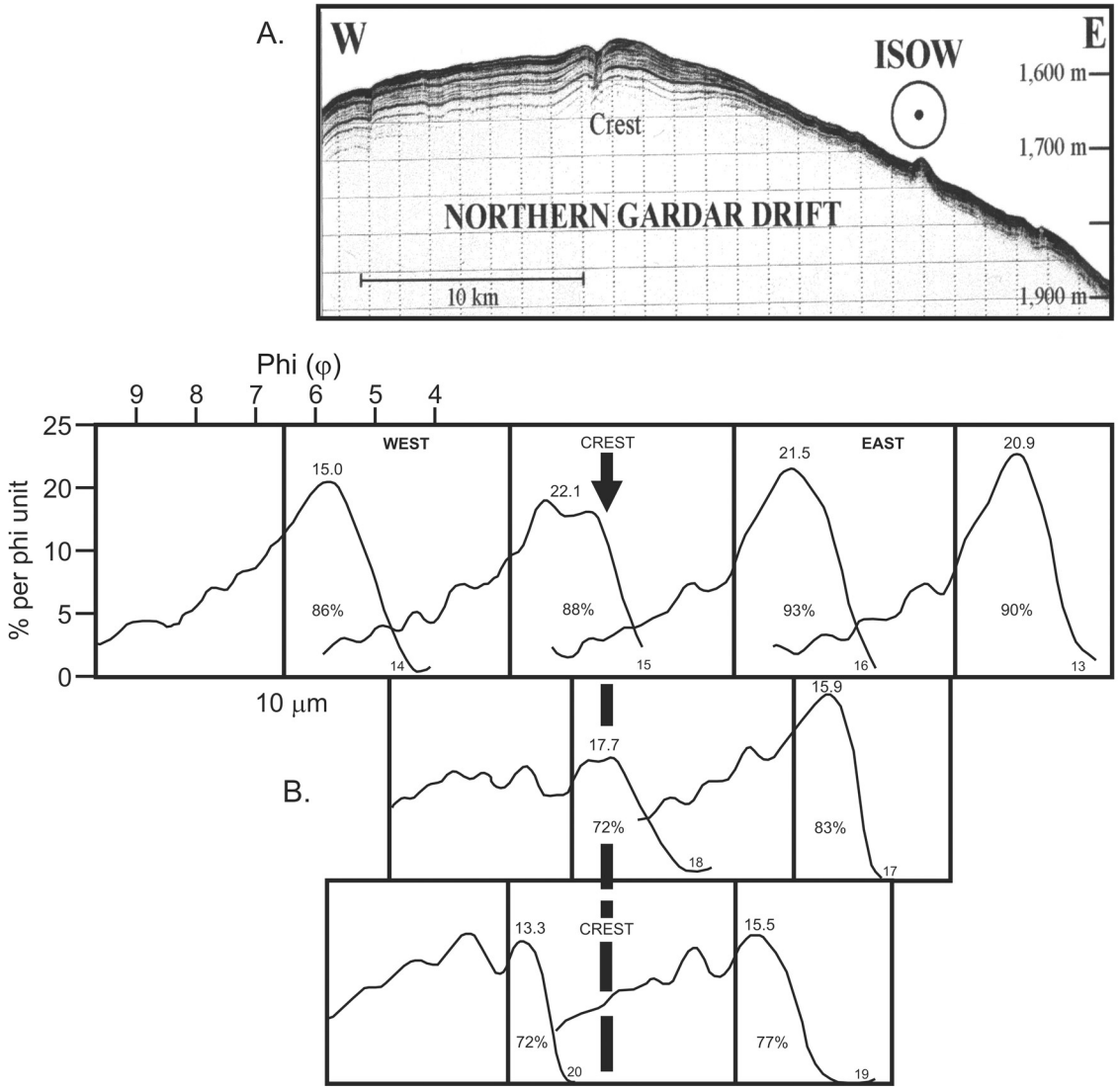

Figure 12. (a) The 3.5 kHz record over northern Gardar Drift showing variation in reflector spacing indicative of slower sedimentation rate on the east side and faster on the west due to flow speed variation [from *Bianchi and McCave*, 2000]. (b) Variation in size on three transects across Gardar Drift (data from *Bianchi and McCave* [2000]). Shown are size spectra with the SS mean size above the peak and the percentage of total silt under the curve, both generally bigger on the east side. Small numbers on the *x* axis are stations. The vertical line on each curve marks 10 μm.

had been constant. It is thus essential to have good 3.5 kHz profiler and seismic data to assess such potential problems. These complications may not be confined to grain size alone but also occur in other proxies.

4.5. Spatial Aliasing by Movement of Currents Upslope or Downslope

[28] With changing climate comes changing density of water masses participating in the deep circulation. Several records have demonstrated the change from dominance of "North Atlantic Deep Water" (NADW) to "Antarctic Bottom water" (AABW) between interglacials and glacials. If, for example, at the LGM there were convection of relatively fresh water south of the Polar Front as the only northern source to the WBUC, it would be less dense than the present cocktail of NADW sources and likely to be shallower. At a given deep location the time trend in flow speed from glacial to interglacial would be a decrease, while at a shallow point the opposite would occur, possibly with little overall change in Meridional Overturn-

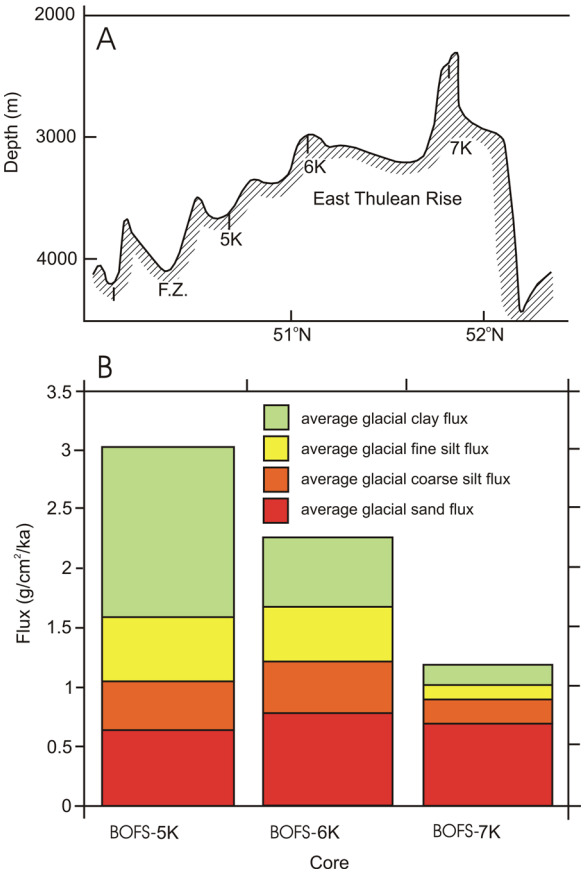

Figure 13. East Thulean Rise, 52°N, 20°W. (a) Topography and core sites and (b) sedimentation rates of different size fractions in cores BOFS-5K to -7K. (After *Manighetti and McCave* [1995]).

ing Circulation (MOC) strength. Study of only the deep section could lead to serious error. This emphasizes the need to study depth transects with flow speed proxies in conjunction with water mass tracers and density (T/S) proxies as well. A few studies have looked at this in some detail on the central N. American margin (see also section 5.2) [*Ledbetter and Balsam*, 1985; *Haskell et al.*, 1991; *Yokokawa and Franz*, 2002], with all concluding that there have been shifts in the focus of current activity. In particular, *Haskell et al.* [1991] show that the major flow on Blake Outer Ridge was shallower than 2900 m prior to ~14 ka back to the LGM.

4.6. Normalization by Subtraction of Signals Relative to an Input Function: IRD

[29] Early in SS investigations of flow speed it was recognized that in some areas variations in size might be due to input variations, independent of variation in bottom currents, and that these would be most likely in sites where vertical input dominated over reworking [*Manighetti and McCave* [1995] (hereafter MM'95) and *McCave et al.* [1995b]. The glacial Northeast Atlantic was such a site, receiving variable input of ice-rafted detritus (IRD). The problem of current inference in this setting was approached by first identifying the grain size characteristics of the input flux through time at a site which was argued to be unaffected by current winnowing or focusing. Grain size changes in sortable silt from current-influenced sites were then calculated by difference from the grain size at the "unaffected" input flux site. The resulting variation in differential grain size was attributed to fluctuating current speed. The necessary detailed correlation between cores was achieved via magnetic susceptibility and lithology.

[30] The cores studied by MM'95 from the isolated East Thulean Rise (51°N, 22°W) (BOFS 5K, -6K and -7K) lie close together and are located well away from potential changes in size due to input of continental detritus and from the axes of major currents. Thus the size characteristics of the sediment should, unless current-modified, reflect the pelagic flux in the area. However, the three sites differ quite markedly in both sedimentation rate, averaging 2.1–5.2 cm kyr^{-1} between the last glacial maximum (LGM) and present, and in terrigenous size distributions. Core BOFS 7K is on the exposed crest of the rise, whereas BOFS 5K is situated in a hollow downslope. The glacial noncarbonate flux at cores 5K and 7K appears to differ in opposite respects (5K high and 7K low in fines), as if the high flux at 5K were a result of accumulation of material winnowed off high places such as 7K (Figure 13). The coarse fraction accumulation rate is much less variable than the fines, suggesting that a process affecting only the fines rather than mass movement causes the redistribution. Core BOFS 6K is from an intermediate topographic position on a gentle local high, and the observed flux lies between that of 5K and 7K. MM'95 argued that the site was unlikely to be subject to either extensive winnowing or focusing of sediment, and was therefore the best recorder of average unmodified input flux because it accumulated "a sediment sequence unmodified by either bottom currents or topographic focusing." It can therefore be used as a "standard" pelagic site to define the characteristics of the input flux. The ideal of defining an input function in terms of a mass flux in different size classes for each core site

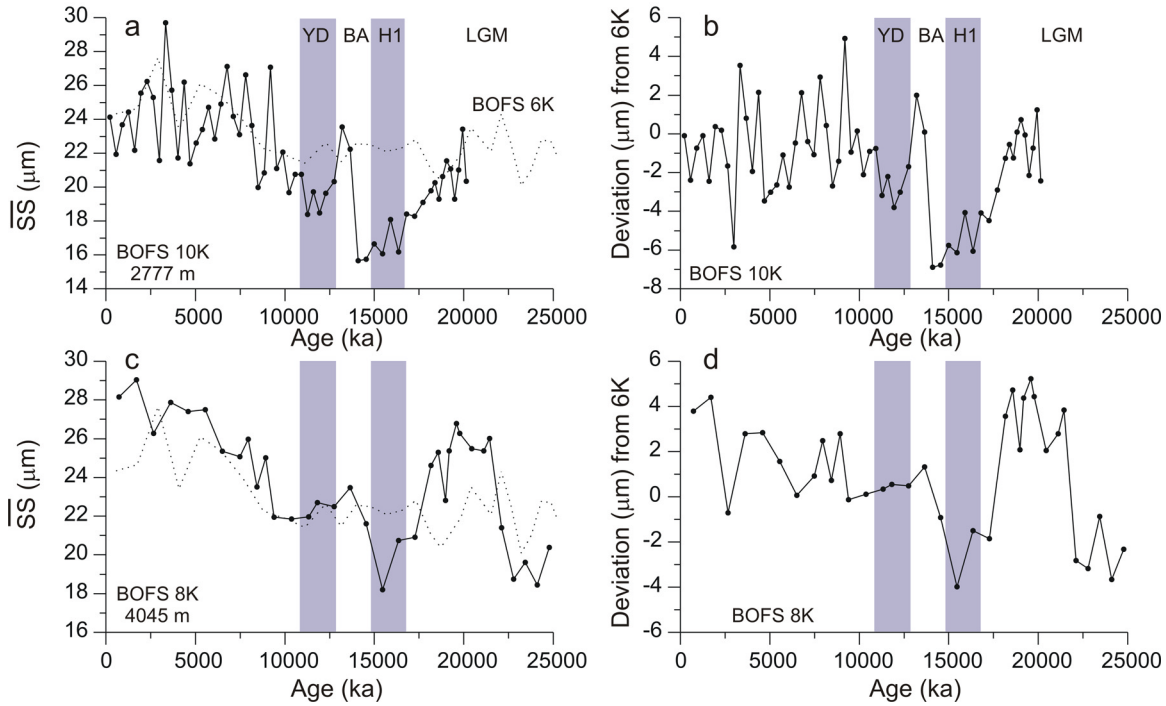

Figure 14. Grain size data for core sites BOFS -8K and -10K immediately north of East Thulean Rise: (a and c) Raw $\overline{SS}$ and (b and d) differential grain size ($\Delta\overline{SS}$) for each site, i.e., $\overline{SS}$ minus the size for BOFS 6K, which is shown as a dotted line in Figures 14a and 14c. (After *Manighetti and McCave* [1995]).

individually was seen as impossible, but using an appropriate standard location (i.e., BOFS 6K) one might set out the expected relative changes downcore in the different fractions at nearby locations, so that deviations due to current sorting could be recognized. It was argued that the size distribution of the glacial input would be constant ("it is likely that the input flux of finer material by ice rafting also varies proportionately to input of the coarsest material" MM'95).

[31] Examination of the raw and differential records (Figure 14) suggests that little was gained from the subtraction procedure, the major features being present in the original records, and niggling doubts remain. Is it reasonable to suppose that the sediment at 6K was really unaltered when there was winnowing above and focusing below? Does it not simply sit conveniently between obviously winnowed and focused sediments but with no further solid justification for being "unaltered"? (On the other hand, the 6K grain size record does not show the current influenced features of those clearly under strong flow, 8K and 10K.). Is the procedure of simple subtraction of mean sizes valid? Should one not take the two whole size distributions and look at their differences in the SS range? Maybe the difference in the means ($\Delta\overline{SS}$) is a suitable index, but it is not obviously so, and it could not be related to a calibration function of the type shown in Figure 1 to get flow speed.

4.7. More Approaches to IRD Problems

[32] In order to extract a current signal from severely IRD affected sediments, *Hass* [2002] performed a correlation between sand percentage and $\overline{SS}$, then subtracted the sand-associated part of $\overline{SS}$ from the original time series (Figure 15a). The underlying assumption is that the sand is not moved by the current and so is an index of the amount of IRD, and that the shape of the size distribution is constant. In this case the sand percentage is proxy for the amount of a constant size distribution diluent which, when subtracted, leaves the current-affected part of the distribution's mean size. As may be seen from Figure 13 there is a lot of scatter around the line. There must be an assumption that, for this data set at least, $\overline{SS}$ increases in size with percent IRD. If the IRD followed a Rosin-Rammler/Weibull type distribution for crushed material, one would expect more sand to be accompanied by more silt. Also if, as is normally the case, the material had a flat weight

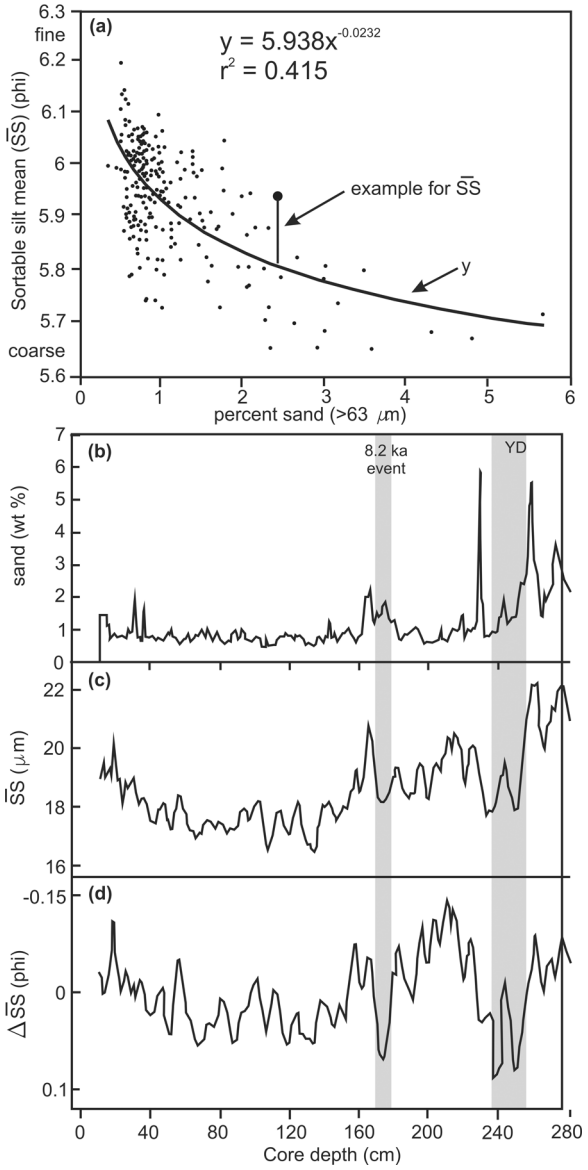

Figure 15. (a) Correlation of $\overline{SS}$ with sand percentage for the Fram Strait area [*Hass*, 2002]. Deviations of $\overline{SS}$ from the line ($\Delta\overline{SS}$) are presumed to have the effect of IRD on the SS mean size removed. (b–d) Time trends in core PS-2837 from Yermak Plateau, east side of Fram Strait: (b) % sand, (c) raw $\overline{SS}$, and (d) $\Delta\overline{SS}$ enhancing the $\overline{SS}$ signal by the subtraction procedure shown above in Figure 15a. YD and 8.2 ka events become more apparent but are present in the original data [from *Hass*, 2002].

(volume) distribution between 10 and 62.5 μm, its (logarithmic) mean size would be 25 μm. SS mean sizes tend to fall in the region 15–30 μm, so the IRD silt would not be hugely distorting, but would put in more coarse silt than is usually found. Thus Hass's empirical correlation has some basis. Nevertheless, the major features of the record are also present in the original record which the subtraction procedure has enhanced. If the procedure of MM'95 is somewhat dubious then this is equally so, even though it appears to produce an intriguing record of flow out of the Arctic [*Hass*, 2002; *Birgel and Hass*, 2004], with flow reductions at the Younger Dryas and 8.2 ka events (Figures 15b–15d).

[33] Large fluxes of IRD pose the problem that the current may not be able to rework the material sufficiently rapidly to impose its characteristics on the size distribution. The rate in Hass's core PS 2837-5 is around 20 cm kyr^{-1} or 2 mm per decade and the rates of MM'95 cores are less than 10 cm kyr^{-1}. Currents of moderate strength, $\sim$15 cm s^{-1} for a few days a year, would be able to process this material. Only if severely episodic dumps of sediment occur, several cm in a year, would these currents be unable to cope. Data shown by *Austin and Evans* [2000] for two periods in the Pliocene and early Pleistocene from south of Iceland where % IRD > 125 μm is up to 50% suggest little effect of IRD on the SS speed proxy (Figure 16). These authors show a well marked peak in speed in the Pliocene record in MIS 103, a warm stage with significant IRD (their Figure 4). However, the strictures of *McCave et al.* [2006] regarding laser data are applicable to this data set. In particular the SS% is very high (50–60%) which is probably accompanied by too-high values of $\overline{SS}$.

[34] Our conclusion regarding IRD is that strong currents are capable of creating a current-sorted signature in IRD just as they are in material removed from debris flows and turbidites. However, the problem lies in our not knowing well the two critical rates, rate and temporal pattern of input and current flow rate. When flow speed is high ($\sim$10 cm s^{-1}) input rates of up to 10 cm kyr^{-1} can easily be reworked. The pitfall of circularity (you need to know the flow speed which you are trying to infer. . .) must be evident to all. It may be that if a credible IRD end-member size spectrum could be identified via the inverse models of *Weltje* [1997], then it could be subtracted from each analysis with recalculation of the sortable silt size values.

4.8. Inverse ("End-Member") Modeling of Grain Size Distributions for Reconstructing Flow Speeds and Sediment Dispersal Patterns

[35] The inverse dissection of grain size distributions into distinct components reflecting combina-

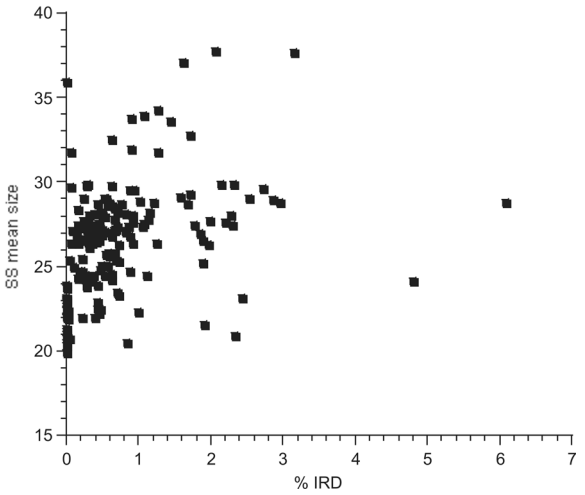

Figure 16. *Austin and Evans* [2000] data from ODP Site 984 south of Iceland (MIS 77–79 and 103): mean sortable silt size (10–63 μm) (by laser) versus IRD (noncarbonate% >125 μm). Due to the laser shape effect the SS% is high in these records; nevertheless, there is little correlation between IRD and $\overline{SS}$ (r = 0.028 or, without two very high IRD values, r = 0.366).

tions of parent end-member populations and transport process-related components has a long history, reviewed most recently by *Weltje and Prins* [2003]. Different compositional or transport components of pelagic sediments can be isolated by fitting multicomponent lognormal (or other) distributions [e.g., *Sun et al.*, 2002]. Computer programs (e.g., "Peakfit") enable this dissection. Recently, a variant of factor or principal component analysis has been used to extract statistically defined end-members from spatial or temporal ensembles of grain size distributions [*Weltje*, 1997]. In this way "end-members" (EM) are defined without requiring individual distributions to represent predetermined end-members, as is the case in the analysis of foraminiferal populations for example. The end-member modeling procedure has been applied to several data sets [*Prins and Weltje*, 1999; *Prins et al.*, 2002; *Stuut et al.*, 2002]. The data are necessarily obtained by laser sizer (with its attendant size biases) because this is the only way of obtaining a wide spectrum (1–1000 μm) analysis by a single method. Having extracted end-members they must be interpreted. EMs from the *Weltje* [1997] algorithm are the numerically most parsimonious, but do not necessarily coincide with the actual real world distributions.

[36] Only one of the applications of the EM technique has been used to make inferences of flow speed and identify an IRD end-member. *Prins et al.* [2002] have applied the EM method to core DS97-2P from the Reykjanes Ridge. Ice-rafted detritus and current-controlled components were postulated (Figure 17). One might expect "pure" (unaffected by fluid flow or mass flow influences) IRD distributions to be similar to the Rosin-Rammler (or Weibull) distribution based on fracturing of grains [*Rosin and Rammler*, 1933; *Kranck and Milligan*, 1985; *Turcotte*, 1997]. Arguably this is given by the size of subglacial till, though marine samples contain less of the coarser (gravel) components than till. This material typically has a flat distribution by volume/weight, or a cumulative particle number distribution of $N = Ad^{-D}$ where D is the fractal dimension of close to 3 [*Turcotte*, 1997, p. 43]. It might seem a little surprising that the Reykjanes Ridge sediments of core DS97-2P yield *two* end-members containing sand over 100 μm (Figure 17). This size must be ice-rafted, so both EM-2 and -1 were assigned an IRD origin by *Prins et al.* [2002], although the amount >100 μm in EM-2 was very small. Comparison of EM-2 (Figure 17) with Figure 2c shows that its strong mode at 23 μm conforms very well to a current sorted signature. The fact that EM-2 contains some 100–200 μm sand may be a statistical artifact or it may be due to biological mixing (upward pumping) of a coarse component, as is found on the Nova Scotian Rise [*McCave*, 1985, 1988]. Similarly it is difficult to see how 2.5 μm clay and 8 μm fine silt modes (EM-3 and -4) both of which must be finer in hydrodynamic terms than indicated by the laser sizer [*McCave et al.*, 2006] can be ratioed to yield a meaningful flow speed index. Both must be components of the floc-deposited distribution [*Curran et al.*, 2004]. EM-1 is clearly IRD with a typically flat distribution, occurring downcore only at positions where sand percentage exceeds 4%.

[37] The EM method relies on accurate assignment of the causal factor(s) underlying particular components and seeing how they increase and decrease relative to others. The EMs suffer from the "locked data" problem of percentages that, given only 3 or 4 EMs, if one goes up, one or all of the others must go down, and so misleading trends of ratios appear possible. It is inherent in the method of decomposition that an end-member will have fixed characteristics so that the modal diameter does not shift, as it does in the sortable silt mean size method. However, by recognizing two wind-blown dust EMs of differing modal size off W. Africa, *Weltje and Prins* [2003] construct a map of the dispersal

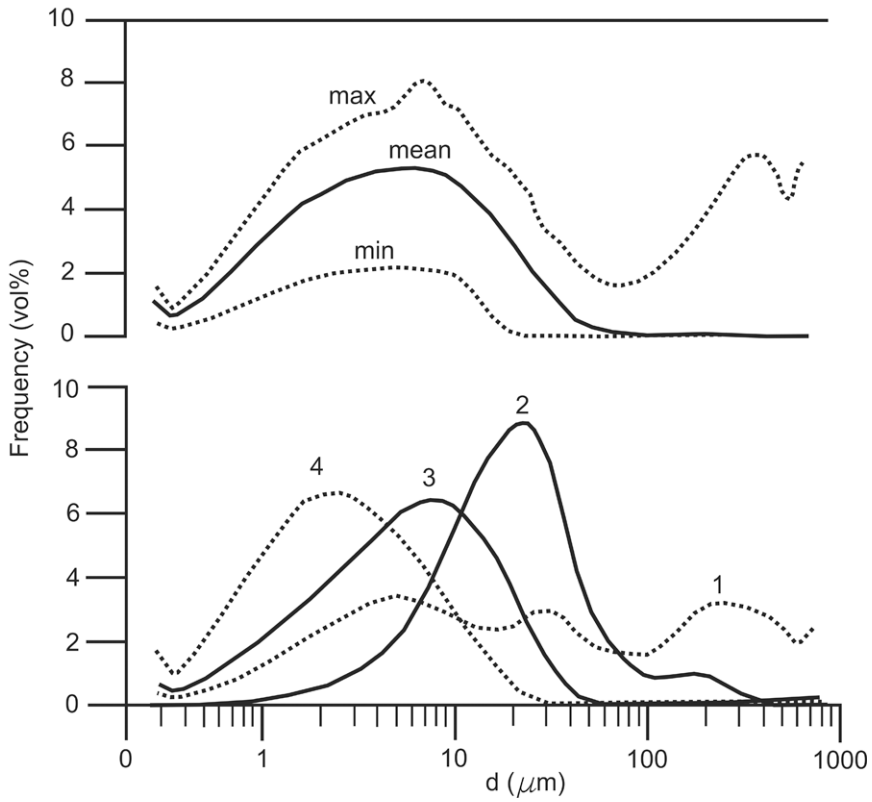

Figure 17. End-member dissection of size distributions from Reykjanes Ridge by *Prins et al.* [2002] (top) Mean size distribution and maximal range of volume frequency measured by laser sizer for each size class (441 samples). (bottom) Modeled end-members according to four-EM model, accounting for 84% of the variance. Both EM-1 and -2 were assigned to an IRD origin.

pattern of wind blown dust expressing its downwind fining tendency based on ratios.

5. Examples of Use of SS Data in Combination With Other Proxies

[38] Over the past decade, much valuable information about past ocean circulation has been inferred from reconstructions of deep ocean flow speed employing the SS proxy. Such work has established the importance of the $\overline{SS}$ as a tracer and complement to the geochemical approaches classically used to infer flow patterns and mixing of subsurface water masses. Initial $\overline{SS}$ studies [e.g., *Wang and McCave*, 1990; *Robinson and McCave*, 1994; *McCave et al.*, 1995b] focused on sediment cores recovered from contourite drift deposits in the North Atlantic, aiming to reconstruct broad scale changes in the flow of NADW during the late Quaternary. This work has now been applied to all major ocean basins, and has been extended in time throughout the Neogene. Consequently, rather than providing an exhaustive review of SS studies we offer an illustrative account of $\overline{SS}$ application using selected records.

5.1. Glacial to Interglacial Changes in the NE Atlantic

[39] The production of NADW and its export to the Southern Ocean have been identified as a major control in the meridional heat and salt transfer between the Northern and Southern Hemispheres. The long-term behavior of the sources of NADW has been investigated in detail through (geochemical) analysis of deep-sea cores at many sites [e.g., *Boyle and Keigwin*, 1982; *Raymo et al.*, 1997]. Such data have shown that the production of Lower (L)NADW was suppressed during glacials, which severely reduced the meridional heat transport and thus amplified the Pleistocene glaciations [*Raymo et al.*, 1990]. Physical evidence for changes in deep ocean circulation on these timescales has also been sought. Regardless of the merits (as discussed in section 3.2) of using a flow speed parameter calculated by difference from a time series of assumed input flux, the reconstructions of

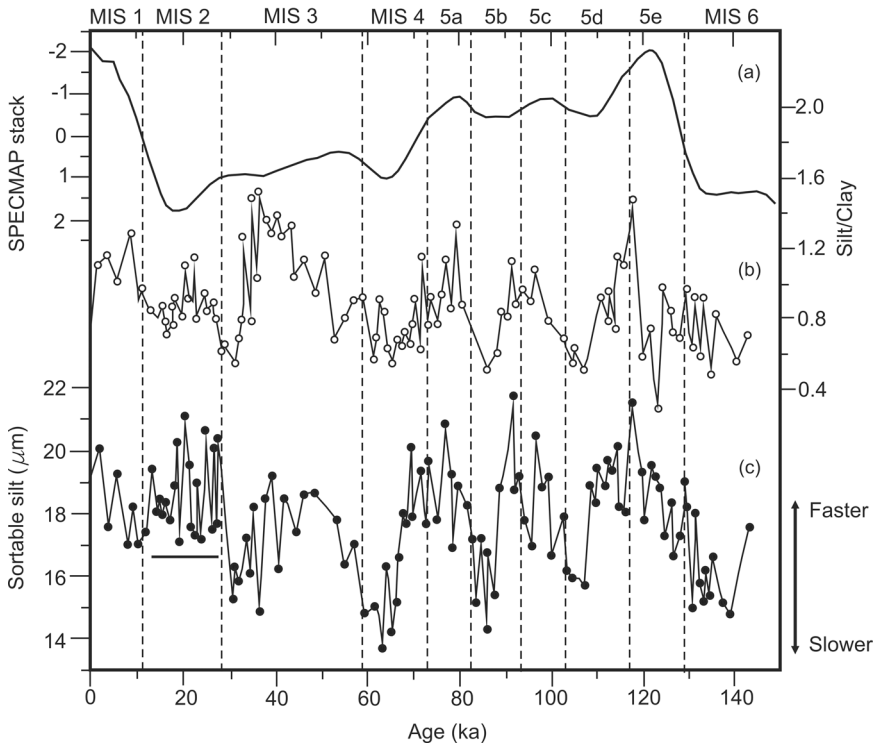

Figure 18. Sedimentological parameters for core MD95-2040 on the Iberian margin plotted against age [*Hall and McCave*, 2000]. (a) SPECMAP stack of benthic δ^{18}O values [*Martinsson et al.*, 1987]. (b) Terrigenous silt/clay ratio (wt% 2–63 μm/wt% <2 μm). (c) $\overline{SS}$; the line under the data in stage 2 indicates the part of the record believed to be unreliable as a current indicator because of possible downslope contamination. The vertical dashed lines indicate the boundaries between Marine Isotope Stages (MIS) achieved by correlating the benthic isotopic record for the core to SPECMAP. Note the clear relationship of slower flow in cold/cool periods from stages 6 to 3 with a lag of a few thousand years relative to isotopic shifts.

MM'95 and *McCave et al.* [1995b], based on the Biogeochemical Ocean Flux Study (BOFS) suite of cores, between 50–60°N and 15–25°W, and ranging in water depth between 1100–4045 m, remain the spatially most comprehensive attempt at examining differences between last glacial and Holocene paleocurrents in the North Atlantic. These data were the first to provide physical confirmation that during the last glacial maximum, the flow of LNADW was slower than in the Holocene and that this was followed by alternating flow increases (early deglacial, Bølling-Allerød, early Holocene) and decreases (Heinrich-1, Younger Dryas) (Figure 14). Comparison of Figure 14 with the recently published Pa/Th flow records of *McManus et al.* [2004] and *Gherardi et al.* [2005] shows them to be remarkably similar.

[40] The $\overline{SS}$ record of core MD95-2040 (40°34.91′N, 09°51.71′W; 2465 m water depth, Figure 18) from the Iberian Margin [*Hall and McCave*, 2000] is currently the most unambiguous record of LNADW flow variability spanning the last glacial-interglacial cycle. The record clearly indicates faster flow during the warm periods and slower in cold, with the $\overline{SS}$ maxima and minima well resolved with respect to the measurement errors. The MD95-2040 record is also important as it serves as an excellent example of the difficulties of paleocurrent reconstruction in a continental margin setting. As is apparent in Figure 18c the $\overline{SS}$ data are anomalously high during MIS 2, and distinctive in that they are coincident with low $CaCO_3$ abundances and very high sediment accumulation rates [cf. *Hall and McCave*, 2000, Figure 4]. The SS data in the MIS 2 portion of the record were considered unreliable by *Hall and McCave* [2000] due to a possible unsorted source effect, i.e., an overwhelming downslope delivery of material that could not be sorted by the slow flow speeds.

5.2. Gardar Drift and Bermuda Rise at the Penultimate Glacial Termination

[41] Records from two cores from different North Atlantic basins, but both under the influence of

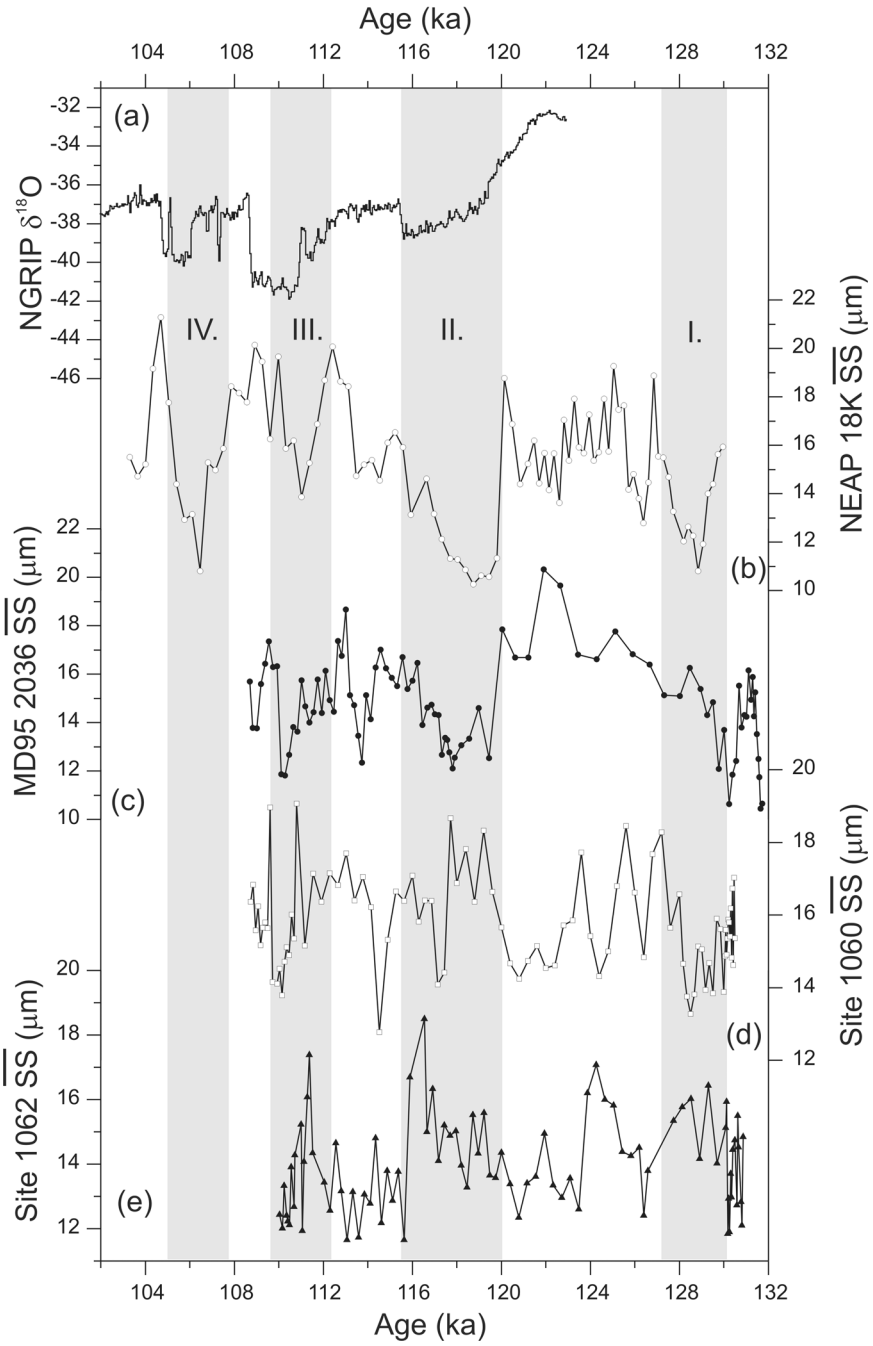

Figure 19. Near bottom $\overline{SS}$ current flow speeds for (b) NEAP 18K (Gardar Drift): (c) MD95-2036 (Bermuda Rise) from *Hall et al.* [1998] together with similar data from (d) ODP Site 1060 and (e) ODP Site 1062 (both Blake-Bahama Outer Ridge) from *Bianchi et al.* [2001]. Also shown for comparison is (a) the $\delta^{18}O$ record from NGRIP [*North Greenland Ice Core Project Members*, 2004]. The gray bands numbered I to IV distinguish events of deceleration followed by acceleration which, on the basis of independent age models for the two sites in Figures 19b and 19c, match very closely in time, demonstrating coordinated flow changes across the North Atlantic [*Hall et al.*, 1998].

NADW flow, one close to its origin and the other down-stream in its evolution are illustrated here (Figures 19b and 19c). The first is from (NEAP 18K, 52°46′N, 30°20.7′W, 3275 m water depth) at the southern extremity of Gardar Drift. This was deposited from Iceland Scotland Overflow Water (ISOW) in the Iceland Basin [*Bianchi and McCave*, 2000] but was covered by Southern

Source Water (SSW) at the LGM [*Bertram et al.*, 1995]. Core MD95-2036 was taken from eastern Bermuda Rise (33°41.4′N, 57°34.5′W, 4462 m water depth), where the sediments are also deposited under current influence [*McCave et al.*, 1982; *Laine et al.*, 1994]. This core is also sited under LNADW at present, with SSW (originally Antarctic Bottom Water) at greater depths over the adjacent Sohm Abyssal Plain (5500 m depth). Because bottom currents exert primary control on sediment deposition and there is negligible interference by direct fall-out from icebergs at either site during the interglacial, they are optimal locations to record bottom water flow changes.

[42] The two cores show several synchronous events (labeled I to IV) in the $\overline{SS}$ record interpreted as deceleration followed by acceleration of the deep current (Figures 19b and 19c). Events II to IV are closely correlated with cooling episodes recorded in the $\delta^{18}O$ of the NGRIP Greenland ice core (Figure 19a). Core NEAP 18K shows an abrupt and large decrease in the $\overline{SS}$ (from about 16 to 11 μm (Figure 19b, event I), indicative of slowing flow speeds, from ~130 ka to 129 ka, just before full stage 5e. A similar flow speed decrease is seen on Bermuda Rise about 1000 years earlier, which is also clearly represented in the hydrographic Cd/Ca record of that site [*Adkins et al.*, 1997]. These termination events [cf. *Hall et al.*, 1998, Figure 3] are important in view of recent concepts that infer a redistribution of heat and salt within the ocean as a means to stimulate or slow down the vigor of the MOC.

[43] Inferred flow speeds at both sites increase rapidly into full interglacial conditions (event I), suggesting strengthening NADW flow. A notable feature in both $\overline{SS}$ records is the sharp decrease in the flow speed seen at about 120 ka reaching a minimum value at ~119–118 ka (event II). During that event between 120 and 118 ka, the abundance of the warm species *N. pachyderma* (d.) in NEAP 18K decreases from 35% to <5% and planktonic $\delta^{18}O$ values increase by ~0.65‰, which, with negligible ice volume effect, suggest a cooling of the northward-flowing surface water temperature of 2 to 3°C. These data indicate that the flow slowed down in an event that marked, if not the end [*Adkins et al.*, 1997], then the beginning of the end of the last interglacial, and which was not clearly marked at this time in any chemical proxy. The flow speed evidence here was the key. However, subsequent flow speed and hydrographic reconstruction of the DWBC on the Blake Ridge and Bahama Outer Ridge (ODP Site 1060, 3480 m water depth and Site 1062, 4760 m water depth; Figures 19d and 19e) by *Bianchi et al.* [2001] suggest that the LNADW production changes inferred at the ~118 ka event were more complex than suggested above and involved an additional vertical migration of the flow axis of the DWBC. This latter observation is important as it highlights the influence of spatial variability of $\overline{SS}$ proxy reconstruction within a DWBC system that, under changing source water production, may vary both its velocity and vertical position in the water column. Such effects can only be recognized by the use of multiple sites forming a depth transect across the current of interest.

[44] This approach was adopted by *Yokokawa and Franz* [2002], who integrated SS measurements and magnetic properties for the interval MIS 10.2–8.3 (350 to 250 ka) using ODP Sites 1055–1062. These BBOR sites provide an intermediate and deep water transect across the DWBC from 1800 m to 4760 m water depths. The data show a similar signal to the DWBC reconstruction of *Bianchi et al.* [2001] with the fast flowing core located >3000 m water depth during interglacial periods and a shoaling to around 2200 m water depth during glacial periods. Through the transitions between these periods, the fast flowing core of the DWBC decreased in depth and its intensity increased. On its own the SS proxy provides no indication of flow direction. *Yokokawa and Franz* [2002] employed the azimuth of the maximum axis of the magnetic anisotropy ellipsoid (K_{max}), as an additional current flow direction indicator. For the BOR overall dominant flow directions inferred for the warm intervals were broadly parallel to the bathymetric contour lines. Interestingly, at the deepest site (Site 1062, 4762 m water depth) the directional data suggest the possibility of changing flow direction between warm and cold periods, but whether this relates to changing mode of particle alignment with speed or an inflow along the western side of the basin is unknown.

5.3. Holocene Iceland-Scotland Overflow Water Variability

[45] The global significance of millennial-scale climate shifts during the last glacial cycle is widely accepted. Several high-resolution paleoclimatic investigations of ice cores [e.g., *O'Brien et al.*, 1995] and marine sediment cores [e.g., *Bond et al.*, 1997] suggest a continuation, although much less

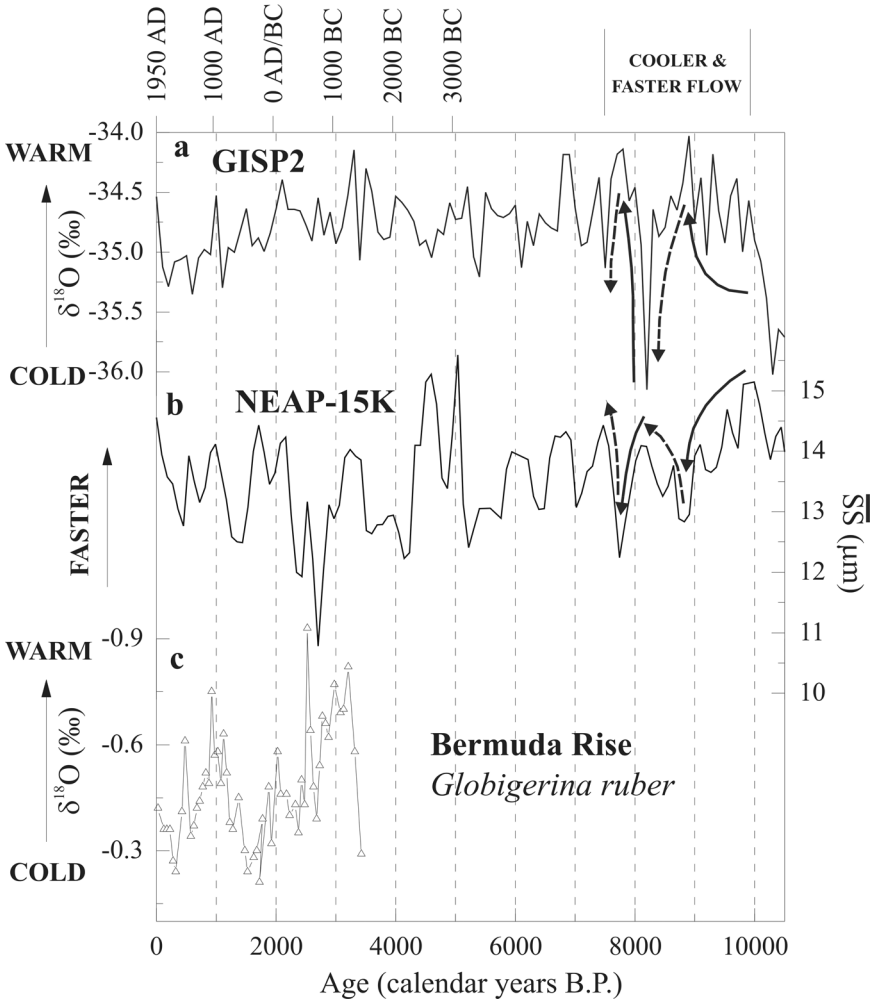

Figure 20. North Atlantic Holocene paleoenvironmental proxy records from *Bianchi and McCave* [1999]. Data are shown on a calendar years B.P. (and AD/BC) basis. (a) δ^{18}O data from central Greenland GISP2 ice core with Gaussian interpolation using a 300-year window. Solid and dashed arrows between 0 and 7.5 kyr B.P. represent periods of general warming or cooling which match relative decreases or increases in the intensity of ISOW flow, respectively. (b) $\overline{SS}$ record for NEAP-15K with Gaussian interpolation using a 300-year window. (c) Planktonic foraminiferal δ^{18}O data from the Sargasso Sea [*Keigwin*, 1996], which mainly reflects changes in sea surface temperature.

distinct, of this variability throughout the Holocene. *Bianchi and McCave* [1999] inferred changes in the current strength of Iceland Scotland Overflow Water (ISOW) from core NEAP 15K (51°07.09′N, 21°52.09′W, 2848 m water depth) recovered from the Gardar drift in the South Iceland Basin. They found evidence for a quasiperiodic ~1500-year variability throughout the Holocene which they also linked, through the northward heat transport in the surface ocean, to climate events in Northern Europe (Figure 20), notably by showing enhanced ISOW flow speeds during the Medieval Warm Period and a subsequent decrease during the Little Ice Age. In addition, a similar Holocene ISOW flow speed record from core NEAP 4K [*Hall et al.*, 2004] located some 1100 km north of NEAP 15K on Björn Drift (61°29.91′N, 24°10.33′W, 1627 m water depth) reports evidence for significant (>95% confidence level) concentration of variance at 1000 and 400 year periods, although the millennial scale cyclicity was poorly defined with additional weaker (>90%) 1400-year and 700-year cycles. Such data are in agreement with evidence of a more prominent 900–1000 year and 400–550 year periodicities in Holocene climate proxies [*Stuiver and Braziunas*, 1989; *Chapman and Shackleton*, 2000; *Schulz and Paul*, 2002; *Risebrobakken et al.*,

2003]. However, we should keep in mind that the identification of spectral peaks in such time series are not without controversy, and a reanalysis of *Bianchi and McCave*'s [1999] data has suggested that the record is better described as containing a spectral continuum without significant spectral lines, possibly related to aliasing of an annual cycle [*Wunsch*, 2000]. Additionally, it is intriguing that in neither NEAP 15K nor -4K do times of reduced ISOW flow speeds coincide with the IRD events described by *Bond et al.* [1997].

[46] Recently, *Ellison et al.* [2006] report results from a multiproxy study of core MD99-2251 recovered from southern Gardar Drift (57°26.87′N, 27°54.47′W; 2620 m water depth). This core is near NEAP 15K and has a mean sediment accumulation rate of ~110 cm kyr^{-1} over the interval of 9,200–7,200 years ago. The data show that the "8.2 ka event" was marked by two distinct cooling events at 8,490 and 8,290 years ago. An associated decrease in $\overline{SS}$ was interpreted as evidence for a significant reduction in ISOW flow speeds. These data provide the strongest evidence yet that surface salinities followed by deep ocean flow changes were forced by meltwater outbursts from a multistep final drainage of the proglacial lakes Aggasiz and Ojibway. Clear identification of these rapid changes is not possible in *Bianchi and McCave*'s [1999] results (even with sedimentation rate of 40 cm kyr^{-1}) and needs the very high sedimentation rates found here to get a signal uncompromised by bioturbation. Of course, ISOW is only one component of the precursor water masses that ultimately comprise North Atlantic Deep Water. Future work should be aimed a providing an integrated reconstruction of each these precursors (i.e., Denmark Strait Overflow Water and Labrador Seawater, as well as ISOW) in order to better identify the dominant modes of Holocene (and older) deep water variability and surface ocean climate in the North Atlantic.

5.4. Flow Into Southern Hemisphere Ocean Basins

[47] Recent work by *Gröger et al.* [2003a] at ODP Sites 927 located on the Ceara Rise in the western equatorial Atlantic (5°27.7′N, 44°28.8′W, 3315 m water depth) found clear evidence for weakened LNADW flow and decreased ventilation during the glacial periods in the time interval 800 ka to 300 ka (MIS 20-8) (Figure 21c). Such a signal contrasts in antiphase with the Southern Hemisphere $\overline{SS}$ record of *Hall et al.* [2001] from ODP Site 1123 (Figure 21b). This site is located on the northeast flank of the Chatham Rise, east of New Zealand (41°47.2′S 171°29.9′W, 3290 m water depth) beneath the southwest Pacific DWBC. The Site 1123 $\overline{SS}$ data in Figures 21a and 21b clearly show faster flow in glacial periods and slower during interglacials over the past 1.2 Myr. Significant spectral peaks were identified at each of the orbital frequencies. These were coherent with benthic records of both oxygen and carbon isotopes at 98% (for 100 and 41 ka) and 90% confidence (for 23 ka). *Hall et al.* [2001] suggest that the pattern of increased glacial DWBC flow speeds was related to greater glacial production of AABW/Circumpolar Deep Water (CDW), a feature supported by the diatom tracer data of *Stickley et al.* [2001] and evidence for a more vigorous glacial flow of CDW seen in the grain size data from cores recovered on a sediment drift south of Shag Rocks passage, in the Drake Passage outflow region [*Pudsey and Howe*, 1998; *Howe and Pudsey*, 1999]. These results resolved the paradox that, although the DWBC has a very large flux, presently it appears to be slow-moving around the New Zealand Margin (shown by current meters, nepheloid layers, bottom photographs), yet there are extensive scours around volcanic pinnacles on the seabed [*McCave and Carter*, 1997] due to the faster flow in the past. In addition, further downstream, these enhanced flows may have produced the circulation changes that drove the glacial increases in sediment focusing recorded in the central equatorial Pacific over the past 300 kyr [*Marcantonio et al.*, 2001]. A clear relationship was also documented between the benthic carbon isotope gradient between Sites 1123 and 849 ($\Delta\delta^{13}C_{(1123\text{-}849)}$) and $\overline{SS}$ with periods of reduced ventilation inferred from the isotopes (high $\Delta\delta^{13}C_{(1123\text{-}849)}$) associated with reduced DWBC flow speeds. Cross-spectral analysis of these records show they are >90% coherent with zero phase lags at the eccentricity and obliquity periods. Such a signal requires a substantial input of nutrient-depleted LNADW to the Southern Ocean during interglacials in addition to the reduced flux of LNADW in glacials, as suggested in the Site 927 data. Waters feeding the Pacific DWBC include LNADW which is modulated by the Antarctic Circumpolar Current (ACC) in the South Atlantic, where these waters are mixed with cold deep waters (Antarctic Bottom waters, AABW) from source regions in the Weddell and Ross Seas and Adelie Coast, to form Circumpolar Deep Water (CDW).

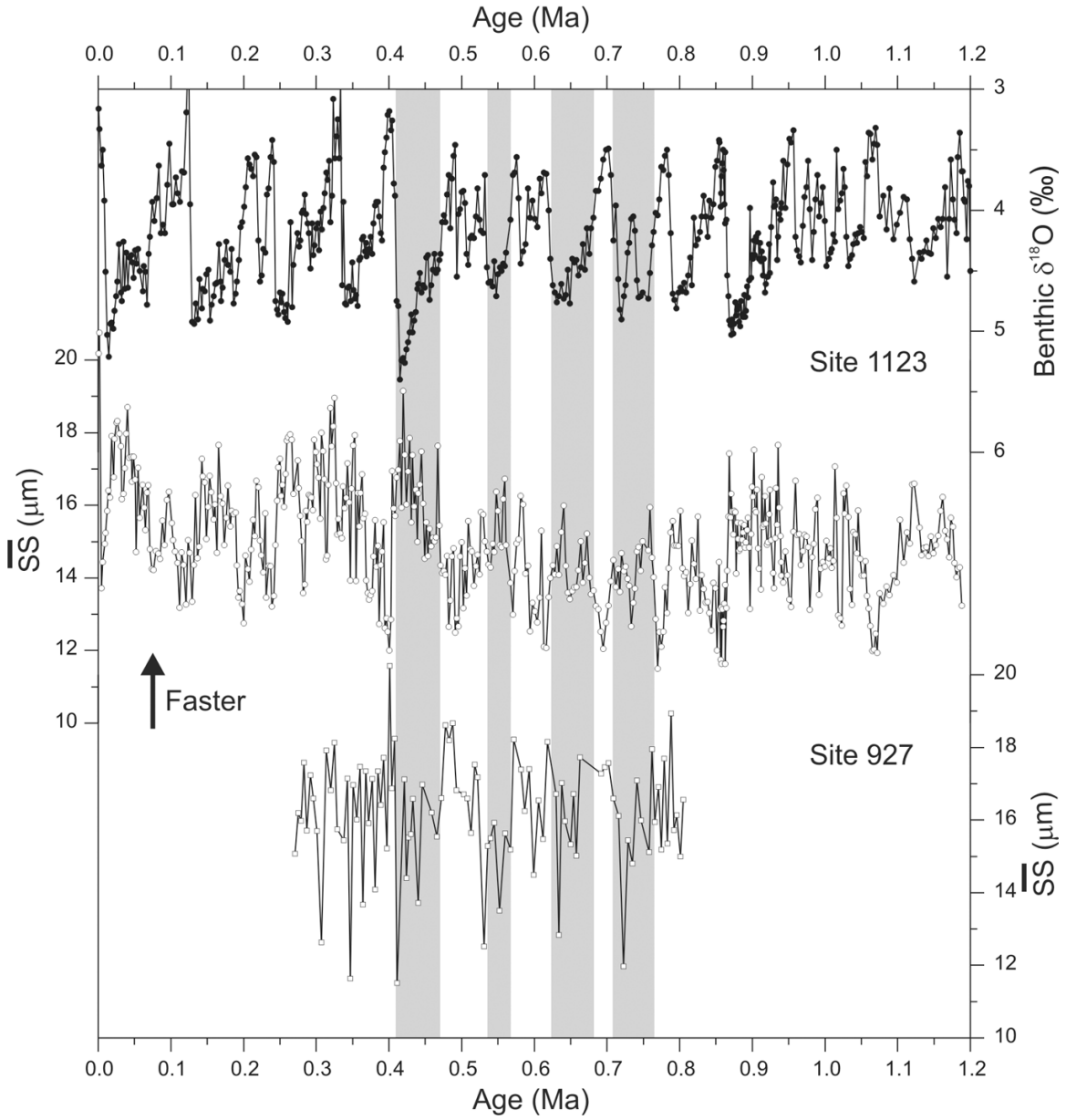

Figure 21. Comparison of the SW Pacific DWBC versus deep flow in the western equatorial Atlantic in the last 1 Myr. (a) Benthic δ^{18}O from ODP Site 1123, Chatham Rise, (b) $\overline{SS}$ at Site 1123 from *Hall et al.* [2001], and (c) $\overline{SS}$ flow speeds from ODP Site 927, Ceara Rise, taken from *Gröger et al.* [2003a]. Gray bands highlight the relationship between glacial $\overline{SS}$ maxima and minima in Sites 1123 and 927, respectively, between MIS 12 and 18.

[48] Cross-spectra between the Site 927 $\overline{SS}$ and benthic δ^{18}O show that minimum flow speeds occur around 7.6 ka after maximum ice volume at the eccentricity period [*Gröger et al.*, 2003b]. In contrast, a similar comparison at Site 1123, over the past 1.2 Myr, found a zero phase lag (of opposite sign) between $\overline{SS}$ and benthic δ^{18}O at the 100 kyr period, and a small lag of 2.1 kyr ± 1.4 kyr at the obliquity period. This suggests a much slower coupling between ice-volume induced changes in LNADW production and the velocity of LNADW in the equatorial Atlantic, than is seen in the southern Hemisphere between AABW production and the flow speed of the DWBC entering the Pacific Ocean. This observation is consistent with the possible strong dependence of AABW production on the winds over the Southern Ocean [*Rahmstorf and England*, 1997].

[49] Although not specifically using $\overline{SS}$ it must be mentioned that the first attempts to relate grain size to relative paleocurrent speeds were in the South

Atlantic [*Ledbetter and Johnson*, 1976; *Ellwood and Ledbetter*, 1977; *Ledbetter*, 1984]. One of the early results of this work was the conclusion that the deep flow of AABW through Vema Channel leaving Argentine Basin was stronger at glacial maxima, similar to the result of *Hall et al.* [2001] for the SW Pacific (but see also section 5.5). Also in the South Atlantic, *Kuhn and Diekmann* [2002] used the abundance of the SS proxy (SS%) to infer flow strength over the past 590 kyr, at 4624 m water depth on the north side of Agulhas Ridge in the S Cape Basin (ODP Site 1089; 40°56.18′S, 09°53.64′E) under a westward deep geostrophic flow [*Tucholke and Embley*, 1984]. The SS% was used in preference to the $\overline{SS}$ in this study because of a suggested modification of terrigenous silt grain-size distribution caused by the removal of biogenic opal required for reliable $\overline{SS}$ measurement. Near bottom waters at Site 1089 are believed to be related to the outflow of the deepest layers of the Weddell Sea. SS% showed well defined glacial-interglacial alternations with more vigorous flow during interglacial periods, suggestive of higher production rates of dense bottom water and invigoration of regional contour currents. *Kuhn and Diekmann* [2002] suggested this variability may be related to the presence of floating ice shelves augmenting deep water formation during high sea level stands. Comparison with the SW Pacific DWBC flow speed record [*Hall et al.*, 2001], which is influenced by a substantially shallower component of CDW than that recorded at Site 1089, may suggest a strong depth related variability in both production and current activity in the Southern Ocean water masses on glacial-interglacial timescales.

[50] Over the past few years oceanographic interest in the Indian Ocean has increased. This is partly because it lies under the path of the so-called "Indonesian Throughflow," which feeds into the S. Equatorial Current, which in turn feeds the Agulhas Current that leaks warm salty water into the South Atlantic. At present only a single paleocurrent study has been published from the Indian Ocean. *McCave et al.* [2005] examined bottom flow through the Madagascar–Mascarene Basin into Amirante Passage over the last glacial-interglacial cycle. These sediments under the DWBC are plastered up against the Madagascar Ridge south of Madagascar, and lie at the foot of Farquhar Ridge north of the island in the entrance to Amirante Passage [cf. *McCave et al.*, 2005, Figures 1 and 3]. Low sedimentation rates hampered high resolution reconstruction at shallow depths, but core WIND 28K in the entrance to Amirante Passage (10°09.23′S, 51°46.15′E, 4157 m water depth, with a sedimentation rate of 4 cm kyr^{-1}) offers an initial indication of glacial-to-interglacial behavior in the major deep inflow path to the Indian Ocean (Figure 22). In general the results, perhaps surprisingly, suggest bottom flows varied only slightly between glacial and interglacials, with faster flow in the warm periods of the last interglacial and minima in cold periods. The dominant feature of the WIND 28K records are four pulses of substantially faster flow that correspond to positive benthic $\delta^{18}O$ shifts of 0.5–1‰. *McCave et al.* [2005] emphasize the correspondence of these pulses to global cooling phases and major falls in sea level, suggesting sharp increases of bottom-water density, and a transient local geostrophic effect. In contrast to the deep inflow to the SW Pacific (shown in Figure 21) peak flow speeds in the Amirante Passage appear limited to the periods of inferred density variation, not to the subsequent periods of uniform higher density (i.e., glacial maxima). *McCave et al.* [2005] conclude that during the inferred periods of density change and high flow speeds, the deep near-bed waters of the Indian Ocean inflow were strongly stratified. This process culminated in the basins filling up with uniformly higher density water, thereby removing the density contrast between the lower inflow and water above, resulting in slower flow speeds in the glacial maxima.

[51] It is of interest and possible significance that *Ledbetter*'s [1986a] reworking of the Vema Channel data indicated that the flow speed maxima also occurred at interglacial to glacial transitions, specifically MIS 7 to 6 and 5a to 4. Like the Indian Ocean Amirante Passage data, this too is from flow through a choke-point. More work is clearly needed in each of the southern hemisphere gateways to characterize the glacial-interglacial, let alone sub-orbital, variation in deep- and shallow-water masses and input strength to the major ocean basins, particularly the depth-related variability in the flow of CDW from the ACC.

5.5. Pre-Quaternary Studies of Flow Variability

[52] Several notable attempts to conduct paleocurrent reconstruction using the SS proxy beyond the Quaternary have been made. Extending their ODP Site 927 Pleistocene time series, *Gröger et al.* [2003b] report evidence for a stepwise reduction of glacial LNADW flow speeds from the late

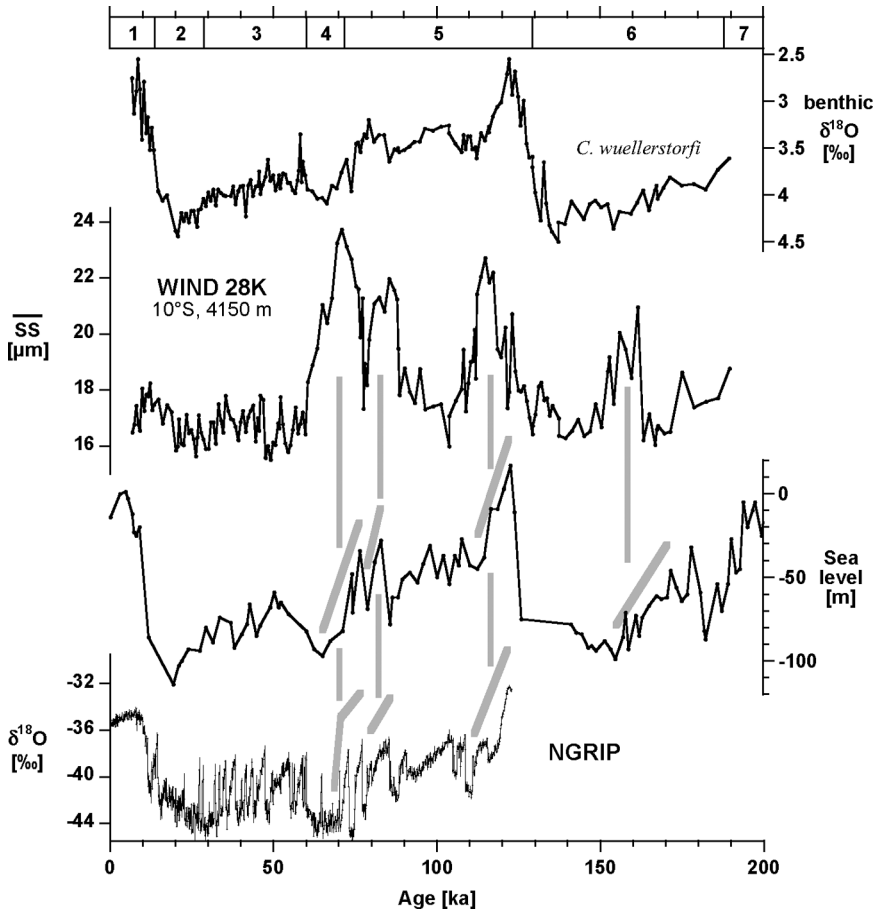

Figure 22. Benthic isotopic (δ^{18}O) and $\overline{SS}$ data for core WIND 28K plotted against age. The sea level curve of *Siddall et al.* [2003] based on core KL-11 from the Red Sea, and the NGRIP Greenland ice sheet δ^{18}O showing large oscillations at MIS 5a [*North Greenland Ice Core Project Members*, 2004] are also given. Heavy gray lines mark the sea level and ice core isotopic shifts corresponding to flow speed transients. After *McCave et al.* [2005].

Pliocene toward the Pleistocene. Of note, they identify a three phase shift in LNADW current strength during the transition from mid-Pliocene warmth to the large-scale Northern Hemisphere Glaciation (NHG) at ~3.2 Ma. Between ~3.5 and 3.2 Ma, LNADW was found to be highly variable with large amplitude fluctuations gradually diminishing and giving way to remarkably stable flow during the initial phase of NHG between ~3.2 and 2.75 Ma. Synchronous with the first occurrence of large-scale continental ice and the marked decrease in convection within the GIN seas, LNADW flow speeds substantially decreases and the high amplitude variability returns. *Gröger et al.* [2003b] and colleagues suggest that because of the high degree of sensitivity of NADW production to changes in surface water salinity, the high-amplitude fluctuations of LNADW circulation prior to ~3.2 Ma are linked to changes in the Atlantic salinity budget, while after 2.75 Ma they are primarily controlled by ice sheet forcing. The cause of inferred stability of LNADW during the Northern Hemisphere cooling between ~3.2 and 2.75 Ma remains unclear.

[53] Orbital control on the dynamics of the deep Pacific inflow has also been confirmed during the period of global ice accumulation associated with the expansion of the East Antarctic Ice Sheet (EAIS) in the middle Miocene from ~15.5 to 12.5 Ma [*Hall et al.*, 2003] (Figure 23). Cyclic variation in $\overline{SS}$ and lithological records from Site 1123 were found to be dominated by the 41 kyr orbital obliquity cycle. This result is perhaps not surprising but clearly indicates a strong coupling between the variability in the speed of the DWBC and high-latitude climate forcing that may have persisted within the MOC for at least the past 15 Myr. Long-term changes in flow speed during the interval also suggest an intensification of the

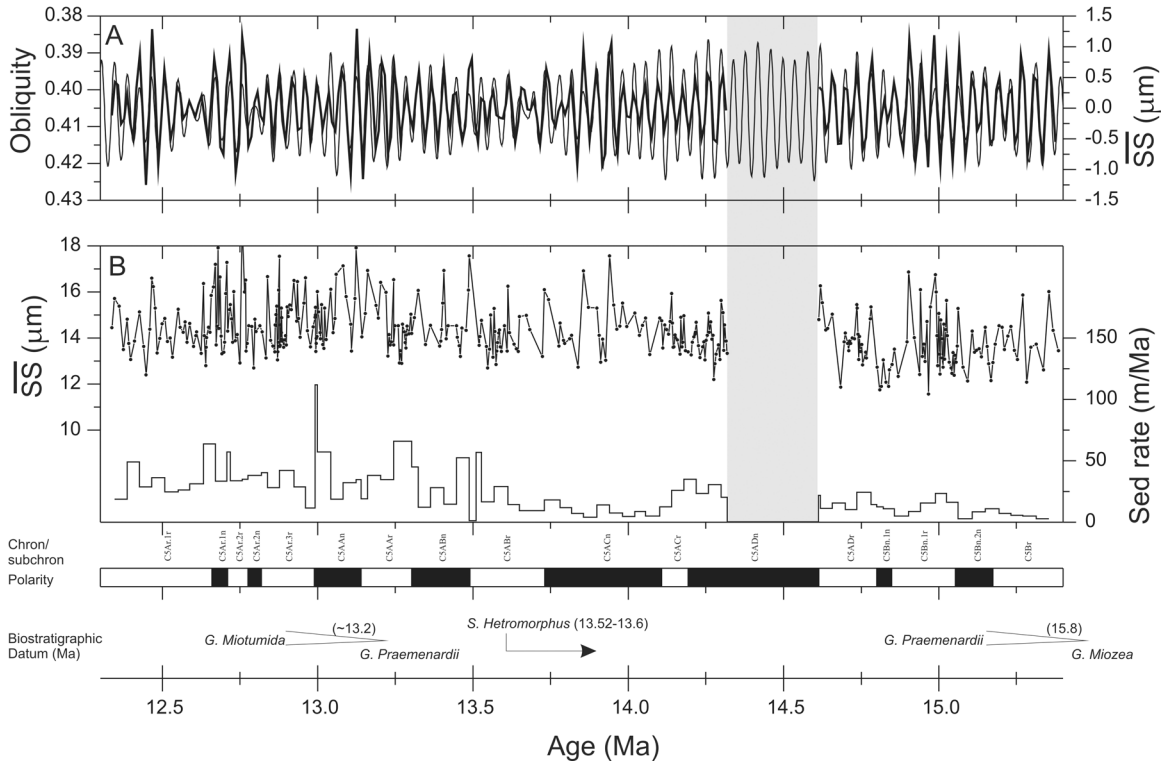

Figure 23. Miocene flow into the SW Pacific from ODP site 1123 from *Hall et al.* [2003]. (a) Comparison of the filtered 41 kyr component of the $\overline{SS}$ with orbital obliquity. The $\overline{SS}$ filter has a central frequency of 0.04065 cycles kyr^{-1} and a bandwidth of 0.01046 cycles kyr^{-1}. (b) $\overline{SS}$ record versus age together with sedimentation rates. Also shown is the polarity record on the 1123 timescale and biostratigraphic datums [*Carter et al.*, 1999]. Shading indicates the time gap at a brief disconformity.

DWBC under an inferred increase in Southern Component Water production. This occurred at the same time as decreasing Tethyan outflow and major EAIS growth between ~15.5 and 13.5 Ma. These results provide the only direct physical evidence that a major component of the MOC was associated with the middle Miocene growth of the EAIS.

[54] Further $\overline{SS}$ evidence that MOC changes were critical to the development of the Neogene ice-house climate are suggested in the prominent shift in ocean circulation recorded at ODP Site 1170 (047°09′S 146°03′E, 2704 m water depth) and ODP Site 1171 (048°30′S 149°07′E, 2148 m water depth) located on the South Tasman Rise at ~24 Ma, just prior (by 50–60 kyr) to the Mi-1 event marking the Oligocene-Miocene boundary (OMB). The $\overline{SS}$ flow speed record from Site 1170 record is shown along with the corresponding benthic δ^{18}O record in Figure 24. The clear increase in $\overline{SS}$ at 24 Ma is taken by *Pfuhl and McCave* [2005] as independent evidence for a strengthening of the west-to-east flow through the Tasman Gateway, which was well known to have opened at ~33 Ma, the Eocene-Oligocene Boundary [*Stickley et al.*, 2004]. This flow speed increase is accompanied by a clear increase in benthic δ^{18}O at the site which, together with additional isotopic evidence from other Southern Ocean sites, is plausibly attributed to the inception of a full, i.e., modern-type, ACC circulation pattern at the OMB. A requirement for the complete establishment of full circumpolar circulation is the tectonic opening of the Drake Passage south of America to deep throughflow. However, the timing of the Drake Passage opening is poorly constrained and there has been considerable debate in the literature over two alternative time ranges based mainly on paleomagnetic tectonic reconstructions [e.g., *Barker and Burrell*, 1977; *Lawver and Gahagan*, 1998; *Livermore et al.*, 2004]. An early Drake Passage opening at ~31–28.5 Ma and a later or younger age range between ~22 and 17 Ma. The combination of $\overline{SS}$ and isotopic data presented by *Pfuhl and McCave* [2005] strongly support a deep DP-opening near the OMB at 23 Ma instead of a

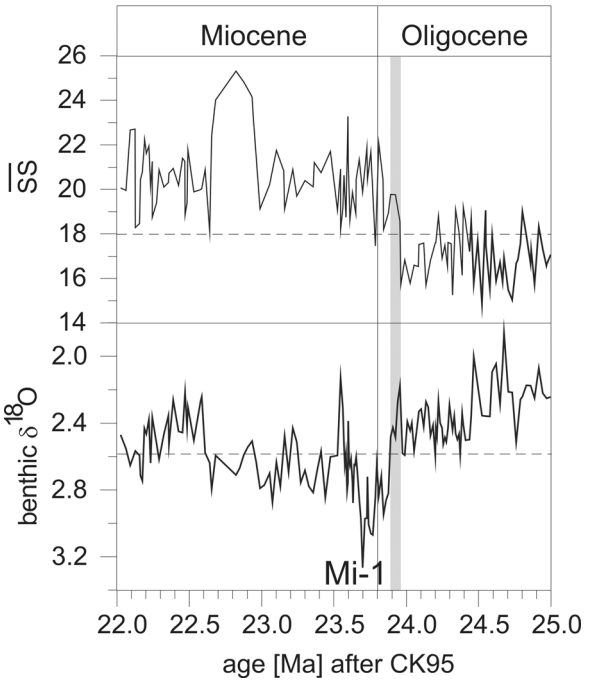

Figure 24. Paired benthic δ^{18}O and $\overline{SS}$ data from ODP Site 1170 plotted against age from *Pfuhl and McCave* [2005]. These data suggest that the increase in current speed at ~23.95 Ma precedes the onset of the Mi-1 event at ~23.9 Ma. (The authors used the *Cande and Kent* [1995] timescale with the Oligocene-Miocene boundary at 23.9 Ma).

much earlier date close to the Eocene-Oligocene boundary.

6. Prospects

6.1. Links With Other Flow/Circulation and Water Mass Proxies

[55] To date there has been insufficient use of more than one flow rate proxy or more than two water mass markers from the same cores. Most work is performed with a background of benthic isotopic data so that, when epibenthic species are used, carbon isotopes provide nutrient-related data [*Mackensen and Bickert*, 1999; *Curry and Oppo*, 2005]. This has been coupled with the phosphate proxy Cd/Ca ratio in benthic foraminifera [e.g., *Boyle and Keigwin*, 1982]. Both are biologically mediated and can define the extent of water masses but do not act as conservative tracers capable of giving water mass mixing information. That now appears possible with the neodymium isotope water mass tracer which is inorganic and has been used in conjunction with carbon isotopes, but not with any flow rate proxy [*Piotrowski et al.*, 2004]. *Kissel* [2005] shows that the concentration of magnetic grains (mainly very fine magnetite) may be interpreted as a proxy for the strength of NADW. This must relate to the erosive power of the LNADW source flows passing over and through the basaltic Greenland-Scotland Ridge where the magnetite is entrained. Although some have claimed a dynamically-related size dependence of the magnetic grains [*Snowball and Moros*, 2003], it is difficult to envisage a hydrodynamic sorting process for such small grains (10 nm–10 μm) that must be deposited in aggregates. It is more likely that the magnetic size covaries with erosion-related parameters at source as suggested by *Moreno et al.* [2002], and mimics the concentration parameter of *Kissel* [2005].

[56] The principal flow rate or ventilation rate proxies are grain size (reviewed here), anisotropy of magnetic susceptibility (AnMS) [*Rees*, 1961; *Hamilton and Rees*, 1970], carbon-14 age difference between surface and bottom waters [*Broecker et al.*, 1990; *Adkins and Boyle*, 1997], ^{230}Pa/^{231}Th$_{xs}$ [*Bacon and Rosholt*, 1982; *McManus et al.*, 2004] and the density field obtained via benthic oxygen isotopes used to make geostrophic calculations of flow [*Lynch-Stieglitz et al.*, 1999]. While several of these have been used together with benthic δ^{13}C, only AnMS and grain size have been used on the same cores in one of the earliest studies in the field [*Ellwood and Ledbetter*, 1977]. Another case produced conflicting results [*Revel et al.*, 1996; *Kissel et al.*, 1997] because of the use by *Revel et al.* [1996] of a laser size analyzer which *McCave et al.* [2006] show to give misleading results in the sortable silt range. The recent uses of the ^{231}Pa/^{230}Th advection rate tracer over the deglaciation from 19 ka to the Holocene [*McManus et al.*, 2004; *Gherardi et al.*, 2005] agrees with the SS grain size tracer in the N.E. Atlantic [*McCave et al.*, 1995b] (Figure 14) but on different cores.

[57] The next step must be to use most of these tracers together on the same set of cores. It is particularly important to use both flow rate and water mass tracers together because there are numerous cases where flow rate changes are inferred but it is not the same water mass whose flow rate changes. Particularly in the N. Atlantic, cores from 3,000 to 4,000 m depth sample NADW in the Holocene, but southern source water at the glacial maximum and alternations between the two end-members during deglaciation. It is essential to

know what happens to the flow rate of each end-member, rather than that one was slow at a certain time while the other was fast at another time. Unfortunately many data sets are of this under-resolved type.

6.2. Calibration and Significance

[58] A considerable hindrance to the application of the SS proxy is that it has yet to be calibrated in terms of flow speed and presently gives only relative changes. The nearest we have so far is *Ledbetter* [1986a] total silt mean calibration of Figure 1. A project is currently underway in which core-top samples have been collected from locations close to long term (>1 year) current metered sites where instruments have been set within 100 m of the seabed (giving the mean and variability of flow speeds from the geostrophic flow just above the boundary layer). Derived properties from the current meter data, such as scalar mean speed, mean and eddy kinetic energy, directional variability, percentage exceedance of speeds above given values which relate to sediment deposition/erosion/winnowing are being correlated with sediment parameters in order to determine relationships. However, the enterprise has encountered problems, such as the meters of WOCE line ICM-3 in the DWBC of the Madagascar Basin having been laid in and around a turbidity current channel. This is a pity because the records are dominated by Rossby waves [*Warren et al.*, 2002] and would provide a useful examination of the mean versus eddy energy problem. New meters are continually being set, e.g., in the UK NERC *RAPID* programme, which should provide new coring targets for this ongoing effort.

[59] Calibration needs to take into account the characteristics of the currents actually affecting sediments. *McCave et al.* [1995a] envisaged several idealized cases of current temporal variability involving different relationships between the mean and eddy components of the flow. Relatively steady slow speeds may remain below the deposition threshold while more variable speeds may go up into the winnowing regime and occasionally into erosion. The scalar speed (rather than vector velocity) is the key parameter to relate to size, but this might not always be directly correlated to net transport. It is clearly important to know whether a change in sediment size is due to mean flow strength (mean kinetic energy, K_M) or variability (eddy kinetic energy, K_E), though in many cases they are positively correlated [*Dickson*, 1983]. Current meter records are often filtered to remove tidal and internal wave frequencies, yet these components may be responsible for critical episodes of sediment resuspension and transport, and thus should be included in any analysis.

[60] Purely on the basis of sedimentary properties we cannot distinguish whether a change in size is due to an increase in the mean speed or an increase in the variability of speed. On the other hand, one can identify those oceanic regions where strong mean flow and those where strong eddy variability is likely to occur [*Dickson*, 1983]. In some regions both signals are found and these may present difficulties in interpretation of sediment. Clearly, an important strategy for the inference of flow speeds bearing on paleocirculation is to sample regions where the eddy K_E is likely to have been relatively low and mean K_M high. Fortunately sediment drifts, favored coring targets because of high sedimentation rates, under DWBCs, tend to have elevated K_M/K_E ratios. The modern surface sediment data of *Ledbetter* [1986b] from the western Argentine Basin, a region of both high K_M and K_E showing a clear mean current-related pattern is most encouraging in this regard. The correlation between K_E and variations in suspended sediment concentration in Argentine Basin, found by *Richardson et al.* [1993] indicates that the sorting events required to produce the current controlled grain size are deep-sea storms, i.e., some variability is needed to yield sorting. Although modern tracer techniques have demonstrated higher levels of abyssal turbulence associated with the topographic roughness of mid-ocean ridges (and lower levels with smoother abyssal plains and continental rise) [*Polzin et al.*, 1997; *Mauritzen et al.*, 2002], ridges are not often the targets of coring for high-resolution paleoceanographic records.

6.3. Downcurrent Fining and the Difficulty of "Absolute" Calibration

[61] It is obvious that if there were no material of, say, 25–40 μm size, the mean size of the 10–63 fraction would necessarily fall in the lower end of the 10–25 μm range. On several sediment drifts the bottom sediments become finer downcurrent along the transport path (e.g., Gardar Drift [*Bianchi and McCave*, 2000]; Blake-Bahama Outer Ridge to Greater Antilles Outer Ridge [*Tucholke*, 1975]). Thus the downcurrent end of the drift could contain a truncated SS fraction with little, if any, very coarse silt. In this case the $\overline{SS}$ value would necessarily be finer than that for the same flow speed at

the upstream end of the drift where such coarser material was present. This raises the questions: (1) does this situation ever occur for fine sediments (i.e., are some sizes actually absent) as it clearly does for sands, (2) if it does not then can downcurrent coarsening occur if flow speed or winnowing increases spatially, as is seen for sands [*McCave*, 1978; *McLaren and Bowles*, 1985] and occasionally for estuarine fine sediments [*Pascoe et al.*, 2002]? If it does, then it would, unfortunately, imply that no absolute calibration of $\overline{SS}$ to flow speed was possible.

7. Concluding Remarks

[62] Grain size proxies for flow speed have the advantage that they are dominated by local conditions but the disadvantage that they do not give an integrated picture of the flux. They are like a single current meter close to the bed rather than the array of meters normally deployed. Nevertheless, the proxy is not mediated by biology, and, on sediment drifts with sedimentation rates much higher than 2 cm kyr^{-1}, it primarily records depositional flow intensity. In well chosen locations this is representative of major deep ocean flows. In common with other proxies, it is susceptible to distortion by down slope sedimentation events on continental margins. Use of the 10–63 μm part of the size spectrum, sortable silt, is justified on empirical and theoretical grounds so as to avoid effects of cohesion in finer sizes. Being grounded in physical sedimentology and sediment transport mechanics, this proxy comes from a less familiar background to many paleoceanographers than those rooted in isotope and trace element geochemistry. It therefore provides an essential complement to the regular paleoceanographic diet.

[63] In the future we expect to see use of several proxies for flow rate and water mass identity on the same samples. Also, the calibration of the $\overline{SS}$ proxy and determination of the part eddy energy plays in generating the signals to give us a "mud current-meter" remains an important item on the agenda.

Acknowledgments

[64] We are grateful to the UK Natural Environment Research Council and its Rapid Climate Change Programme for its support of our work under several grants. Our respective universities have supported us with equipment and laboratory facilities in which the methods described here have been honed. We thank the members of the SCOR/IMAGES Working Group on Past Ocean Circulation (PACE) for useful discussions. We also thank Bill Austin, Giancarlo Bianchi, and M. Groger, who provided data, and Thorsten Kiefer, Helen Pfuhl, and especially Sharon Capon, who made figures. We are grateful for the attention to a long manuscript paid by the editor Laurent Labeyrie and associate editor Catherine Kissel and referees Roger Flood and Anon, whose comments were most helpful.

References

Adkins, J. F., and E. A. Boyle (1997), Changing atmospheric $\Delta^{14}C$ and the record of deep water paleoventilation ages, *Paleoceanography*, *12*, 337–344.

Adkins, J. F., E. A. Boyle, L. D. Keigwin, and E. Cortijo (1997), Variability of the North Atlantic thermohaline circulation during the last interglacial period, *Nature*, *390*, 154–156.

Agrawal, Y. C., I. N. McCave, and J. B. Riley (1991), Laser diffraction size analysis, in *Principles, Methods and Application of Particle Size Analysis*, edited by J. P. M. Syvitski, pp. 119–128, Cambridge Univ. Press, New York.

Austin, W. E. N., and J. R. Evans (2000), Benthic foraminifera and sediment grain size variability at intermediate water depths in the northeast Atlantic during the late Pliocene-early Pleistocene, *Mar. Geol.*, *170*, 423–441.

Bacon, M. P., and J. N. Rosholt (1982), Accumulation rates of Th-230, Pa-231, and some transition metals on the Bermuda Rise, *Geochim. Cosmochim. Acta*, *46*, 651–666.

Barker, P. F., and J. Burrell (1977), The opening of the Drake Passage, *Mar. Geol.*, *25*, 15–34.

Behl, R. J., R. Tada, and T. Irino (2000), Late Quaternary textural changes offshore of Point Conception, Site 1017, Central California margin, *Proc. Ocean Drill. Program Sci. Results*, *167*, 255–261.

Bertram, C. J., H. Elderfield, N. J. Shackleton, and J. A. MacDonald (1995), Cadmium/calcium and carbon isotope reconstructions of the glacial northeast Atlantic Ocean, *Paleoceanography*, *10*, 563–578.

Bianchi, G. G., and I. N. McCave (1999), Holocene periodicity in North Atlantic climate and deep-ocean flow south of Iceland, *Nature*, *397*, 515–517.

Bianchi, G. G., and I. N. McCave (2000), Hydrography and sedimentation under the deep western boundary current on Björn and Gardar Drifts, Iceland Basin, *Mar. Geol.*, *165*, 137–169.

Bianchi, G. G., I. R. Hall, I. N. McCave, and L. Joseph (1999), Measurement of the sortable silt current speed proxy using the Sedigraph 5100 and Coulter Multisizer IIe: Precision and accuracy, *Sedimentology*, *46*, 1001–1014.

Bianchi, G. G., M. Vautravers, and N. J. Shackleton (2001), Deep flow variability under apparently stable North Atlantic Deep Water production during the last interglacial of the subtropical NW Atlantic, *Paleoceanography*, *16*, 306–316.

Birgel, D., and H. C. Hass (2004), Oceanic and atmospheric variations during the last deglaciation in the Fram Strait (Arctic Ocean): A coupled high-resolution organic-geochemical and sedimentological study, *Quat. Sci. Rev.*, *23*, 29–47.

Blumsack, S. L., and G. L. Weatherly (1989), Observations of the nearby flow and a model for the growth of mudwaves, *Deep Sea Res., Part A*, *36*, 1327–1339.

Bond, G., W. Showers, M. Cheseby, R. Lotti, P. Almasi, P. De Menocal, P. Priore, H. Cullen, I. Hajdas, and G. Bonani (1997), A pervasive millennial-scale cycle in North Atlantic Holocene and glacial climates, *Science*, *278*, 1257–1266.

Boyle, E. A., and L. D. Keigwin (1982), Deep circulation of the North Atlantic over the last 2000,000 years: Geochemical evidence, *Science*, *218*, 784–787.

Broecker, W. S., T.-H. Peng, S. Trumbore, G. Bonani, and W. Wolfli (1990), The distribution of radiocarbon in the glacial ocean, *Global Biogeochem. Cycles*, *4*, 103–117.

Brun-Cottan, J. C. (1971), Etude de la granulometrie des particules marines, mesures éfectuées avec un compteur Coulter, *Cah. Oceanogr.*, *23*, 193–205.

Bulfinch, D. L., and M. T. Ledbetter (1984), Deep western boundary undercurrent delineated by sediment texture at base of North American continental rise, *Geo Mar. Lett.*, *3*, 31–36.

Bulfinch, D. L., M. T. Ledbetter, B. B. Ellwood, and W. L. Balsam (1982), The high-velocity core of the western boundary undercurrent at the base of the United States continental rise, *Science*, *215*, 970–973.

Cande, S. C., and D. V. Kent (1995), Revised calibration of the geomagnetic polarity timescale for the Late Cretaceous and Cenozoic, *J. Geophys. Res.*, *100*, 6093–6095.

Carter, R. M., I. N. McCave, C. Richter, and L. Carter (1999), Southwest Pacific gateways, in *Proceedings of the Ocean Drilling Program, Initial Results* [CD-ROM], vol. 181, Ocean Drill, Program, College Station, Tex. (Available at http://www-odp.tamu.edu/publications/181_IR/181ir.htm)

Chang, T. S., B. W. Flemming, and A. Bartholomä (2005), Distinction between sortable silts and aggregated particles in muddy intertidal sediments of the southern North Sea, in *From Particle Size to Sediment Dynamics*, *Rep. 13*, edited by B. W. Flemming, D. Hartmann, and M. T. Delafontaine, pp. 117–119, Res. Cent. TERRAMARE, Wilhelmshaven, Germany.

Chapman, M. R., and N. J. Shackleton (2000), Evidence of 550-year and 1000-year cyclicity in North Atlantic circulation patterns during the Holocene, *Holocene*, *10*, 287–291.

Coakley, J. P., and J. P. M. Syvitiski (1991), Sedigraph technique, in *Principles, Methods and Application of Particle Size Analysis*, edited by J. P. M. Syvitski, pp. 129–142, Cambridge Univ. Press, New York.

Curran, K. J., P. S. Hill, T. M. Schell, T. G. Milligan, and D. J. W. Piper (2004), Inferring the mass fraction of floc-deposited mud: Application to fine-grained turbidites, *Sedimentology*, *51*, 927–944.

Curry, W. B., and D. W. Oppo (2005), Glacial water mass geometry and the distribution of $\delta^{13}C$ of ΣCO_2 in the western Atlantic Ocean, *Paleoceanography*, *20*, PA1017, doi:10.1029/2004PA001021.

Dade, W. B., A. R. M. Nowell, and P. A. Jumars (1992), Predicting erosion resistance of muds, *Mar. Geol.*, *105*, 285–297.

Dickson, R. R. (1983), Global summaries and intercomparisons: Flow statistics from long-term current meter moorings, in *Eddies in Marine Science*, edited by A. R. Robinson, pp. 278–353, Springer, New York.

Ding, Z. L., E. Derbyshire, S. L. Yang, Z. W. Yu, S. F. Xiong, and T. S. Liu (2002), Stacked 2.6-Ma grain size record from the Chinese loess based on five sections and correlation with the deep-sea $\delta^{18}O$ record, *Paleoceanography*, *17*(3), 1033, doi:10.1029/2001PA000725.

Driscoll, M. L., B. E. Tucholke, and I. N. McCave (1985), Seafloor zonation in sediment texture on the Nova Scotian Lower Continental Rise, *Mar. Geol.*, *66*, 25–41.

Dyer, K. R. (1986), *Coastal and Estuarine Sediment Dynamics*, 342 pp., John Wiley, Hoboken, N. J.

Dyer, K. R., et al. (1996), A comparison of *in situ* techniques for estuarine floc settling velocity measurements, *J. Sea Res.*, *36*, 15–29.

Einstein, H. A., and R. B. Krone (1962), Experiments to determine modes of cohesive sediment transport in salt water, *J. Geophys. Res.*, *67*, 1451–1461.

Eittreim, S. L., E. M. Thorndike, and L. Sullivan (1976), Turbidity distribution in the Atlantic Ocean, *Deep Sea Res. Oceanogr. Abstr.*, *23*, 1115–1127.

Ellison, C. R. W., M. R. Chapman, and I. R. Hall (2006), Surface and deep ocean interactions during the cold climate event 8,200 years ago, *Science*, *312*, 1929–1932.

Ellwood, B. B., and M. T. Ledbetter (1977), Antarctic bottom water fluctuations in the Vema Channel: Effects of velocity changes on particle alignment and size, *Earth Planet. Sci. Lett.*, *35*, 189–198.

Embley, R. W., and R. D. Jacobi (1977), Distribution and morphology of large submarine slides and slumps on Atlantic continental margins, *Mar. Geotechnol.*, *2*, 205–228.

Flood, R. D. (1988), A lee-wave model for deep-sea mudwave activity, *Deep Sea Res., Part A*, *35*, 973–983.

Folk, R. L. (1954), The distinction between grain size and mineral composition in sedimentary rock nomenclature, *J. Geol.*, *62*, 344–359.

Frenz, M., K.-H. Baumann, B. Boeckel, R. Hoppner, and R. Henrich (2005), Quantification of foraminifer and coccolith carbonate in South Atlantic surface sediments by means of carbonate grain-size distributions, *J. Sediment. Res.*, *75*, 464–475.

Fugate, D. C., and C. T. Friedrichs (2003), Controls on suspended aggregate size in partially mixed estuaries, *Estuarine Coastal Shelf Sci.*, *58*, 389–404.

Galehouse, J. S. (1971), Sedimentation analysis, in *Procedures in Sedimentary Petrology*, edited by R. E. Carver, chap. 4, pp. 69–94, Wiley-Interscience, Hoboken, N. J.

Gherardi, J.-M., L. Labeyrie, J. F. McManus, R. Francois, L. C. Skinner, and E. Cortijo (2005), Evidence from the northeastern Atlantic basin for variability in the rate of the meridional overturning circulation through the last deglaciation, *Earth Planet. Sci. Lett.*, *240*, 710–723.

Gibbs, R. J. (1967), The geochemistry of the Amazon River system: Part I. The factors that control the salinity and the composition and concentration of the suspended solids, *Geol. Soc. Am. Bull.*, *78*, 1203–1232.

Gibbs, R. J. (1977), Clay mineral segregation in the marine environment, *J. Sediment. Petrol.*, *47*, 237–243.

Gröger, M., R. Henrich, and T. Bickert (2003a), Glacial-interglacial variability in lower North Atlantic deep water: Inference from silt grain size analysis and carbonate preservation in the western equatorial Atlantic, *Mar. Geol.*, *201*, 321–332.

Gröger, M., R. Henrich, and T. Bickert (2003b), Variability of silt grain size and planktonic foraminiferal preservation in Plio/Pleistocene sediments from the western Equatorial Atlantic and Caribbean, *Mar. Geol.*, *201*, 307–320.

Gross, T. F., and A. R. M. Nowell (1990), Turbulent suspension of sediments in the deep-sea, *Philos. Trans. R. Soc. London, Ser. A*, *331*, 167–181.

Gross, T. F., and A. J. Williams (1991), Characterization of deep-sea storms, *Mar. Geol.*, *99*, 281–301.

Hall, I. R., and I. N. McCave (2000), Palaeocurrent reconstruction, sediment and thorium focussing on the Iberian margin over the last 140 ka, *Earth Planet. Sci. Lett.*, *178*, 151–164.

Hall, I. R., I. N. McCave, M. R. Chapman, and N. J. Shackleton (1998), Coherent deep flow variation in the Iceland and American basins during the last interglacial, *Earth Planet. Sci. Lett.*, *164*, 15–21.

Hall, I. R., I. N. McCave, N. J. Shackleton, G. P. Weedon, and S. E. Harris (2001), Intensified deep Pacific inflow and ventilation during Pleistocene glacial times, *Nature*, *412*, 809–812.

Hall, I. R., I. N. McCave, R. Zahn, L. Carter, P. C. Knutz, and G. P. Weedon (2003), Paleocurrent reconstruction of the deep Pacific inflow during the middle Miocene: Reflections of East Antarctic Ice Sheet growth, *Paleoceanography*, *18*(2), 1040, doi:10.1029/2002PA000817.

Hall, I. R., G. G. Bianchi, and J. R. Evans (2004), Centennial to millennial scale Holocene climate-deep water linkage in the North Atlantic, *Quat. Sci. Rev.*, *23*, 1529–1536.

Hamilton, N., and A. F. Rees (1970), The use of magnetic fabric in paleocurrent estimation, in *Paleogeophysics*, edited by S. K. Runcorn, pp. 445–464, Elsevier, New York.

Haskell, B. J., T. C. Johnson, and W. J. Showers (1991), Fluctuations in deep western North Atlantic circulation on the Blake Outer Ridge during the last deglaciation, *Paleoceanography*, *6*, 21–31.

Hass, H. C. (2002), A method to reduce the influence of ice-rafted debris on a grain size record from northern Fram Strait, Arctic Ocean, *Pol. Res.*, *21*, 299–306.

Hollister, C. D., and I. N. McCave (1984), Sedimentation under deep-sea storms, *Nature*, *309*, 220–225.

Holz, C., J.-B. W. Stuut, and R. Henrich (2004), Terrigenous sedimentation processes along the continental margin off NW Africa: Implications from grain-size analysis of seabed sediments, *Sedimentology*, *51*, 1145–1154.

Howe, J. A., and C. J. Pudsey (1999), Antarctic circumpolar deep water: A Quaternary paleoflow record from the northern Scotia Sea, South Atlantic Ocean, *J. Sediment. Res.*, *69*, 847–861.

Hunt, J. R. (1986), Particle aggregate breakup by fluid shear, in *Estuarine Cohesive Sediment Dynamics*, edited by A. J. Mehta, pp. 85–109, Springer, New York.

Johnson, A. G., and J. T. Kelley (1984), Temporal, spatial, and textural variation in the mineralogy of Mississippi River suspended sediment, *J. Sediment. Petrol.*, *54*, 67–72.

Keigwin, L. D. (1996), The Little Ice Age and Medieval Warm Period in the Sargasso Sea, *Science*, *274*, 1504–1508.

Kissel, C. (2005), Magnetic signature of rapid climatic variations in glacial North Atlantic, a review, *C. R. Geosci.*, *337*, 908–918.

Kissel, C., C. Laj, B. Lehman, L. Labeyrie, and V. Bout-Roumazeilles (1997), Changes in the strength of the Iceland-Scotland overflow water in the last 200,000 years: Evidence from magnetic anisotropy analysis of core SU90–33, *Earth Planet. Sci. Lett.*, *152*, 25–36.

Konert, M., and J. Vandenberghe (1997), Comparison of laser grain size analysis with pipette and sieve analysis a solution for the underestimation of the clay fraction, *Sedimentology*, *44*, 523–535.

Kranck, K., and T. G. Milligan (1983), Grain size distributions of inorganic suspended river sediment, *Mitt. Geol. Paläontol. Inst. Univ. Hamburg*, *55*, 525–534.

Kranck, K., and T. G. Milligan (1985), Origin of grain size spectra of suspension deposited sediment, *Geo Mar. Lett.*, *5*, 61–66.

Kranck, K., and T. G. Milligan (1991), Grain size in oceanography, in *Principles, Methods, and Application of Particle Size Analysis*, edited by J. P. M. Syvitski, pp. 332–345, Cambridge Univ. Press, New York.

Kranck, K., P. C. Smith, and T. G. Milligan (1996a), Grain size characteristics of fine grained unflocculated sediments I: 'One-round' distributions, *Sedimentology*, *43*, 589–596.

Kranck, K., P. C. Smith, and T. G. Milligan (1996b), Grain size characteristics of fine grained unflocculated sediments II: 'Multi-round' distributions, *Sedimentology*, *43*, 597–606.

Krumbein, W. C., and F. J. Pettijohn (1938), *Manual of Sedimentary Petrography*, 549 pp., Appleton-Century-Crofts, New York.

Kuhn, G., and B. Diekmann (2002), Late Quaternary variability of ocean circulation in the southeastern South Atlantic inferred from the terrigenous sediment record of a drift deposit in the southern Cape Basin (ODP Site 1089), *Palaeogeogr. Palaeoclimatol. Palaeoecol.*, *182*, 287–303.

Laine, E. P., W. D. Gardner, M. J. Richardson, and M. Kominz (1994), Currents and advection of resuspended sediment along the north eastern Bermuda Rise, *Mar. Geol.*, *119*, 159–171.

Lawver, L. A., and L. M. Gahagan (1998), Opening of Drake Passage and its impact on Cenozoic ocean circulation, in *Tectonic Boundary Conditions for Climate Reconstructions*, edited by T. J. Crowley and K. C. Burke, pp. 212–223, Oxford Univ. Press, New York.

Ledbetter, M. T. (1984), Bottom-current speed in the Vema Channel recorded by particle-size of sediment fine-fraction, *Mar. Geol.*, *58*, 137–149.

Ledbetter, M. T. (1986a), A late Pleistocene time-series of bottom-current speed in the Vema Channel, *Palaeogeogr. Palaeoclimatol. Palaeoecol.*, *53*, 97–105.

Ledbetter, M. T. (1986b), Bottom-current pathways in the Argentine Basin revealed by mean silt particle size, *Nature*, *321*, 423–425.

Ledbetter, M. T. (1993), Late Pleistocene to Holocene fluctuations in bottom-current speed in the Argentine Basin mudwave field, *Deep Sea Res., Part II*, *40*, 911–920.

Ledbetter, M. T., and W. L. Balsam (1985), Paleoceanography of the deep western boundary undercurrent on the North American continental margin for the past 25,000 yr, *Geology*, *13*, 181–184.

Ledbetter, M. T., and D. A. Johnson (1976), Increased transport of Antarctic Bottom Water in Vema Channel during last ice age, *Science*, *194*, 837–839.

Livermore, R., G. Eagles, P. Morris, and A. Maldonado (2004), Shackleton Fracture Zone: No barrier to early circumpolar ocean circulation, *Geology*, *32*, 797–800.

Lonsdale, P., and B. Malfait (1974), Abyssal dunes of foraminiferal sand on Carnegie Ridge, *Geol. Soc. Am. Bull.*, *85*, 1697–1712.

Lynch-Stieglitz, J., W. B. Curry, and N. Slowey (1999), Weaker Gulf Stream in the Florida Straits during the last glacial maximum, *Nature*, *402*, 644–648.

Mackensen, A., and T. Bickert (1999), Stable carbon isotopes in benthic foraminifera: Proxies for deep and bottom water circulation and new production, in *Use of Proxies in Paleoceanography*, edited by G. Fischer and G. Wefer, pp. 229–254, Springer, New York.

Manighetti, B., and I. N. McCave (1995), Late glacial and Holocene palaeocurrents through South Rockall Gap, NE Atlantic Ocean, *Paleoceanography*, *10*, 611–626.

Manley, P. L., and R. D. Flood (1993), Paleoflow history determined from mudwave migration—Argentine Basin, *Deep Sea Res., Part II*, *40*, 1033–1055.

Marcantonio, F., R. F. Anderson, S. Higgins, P. Schlosser, and P. Kubik (2001), Sediment focusing in the central equatorial Pacific Ocean, *Paleoceanography*, *16*, 260–267.

Martinsson, D. G., N. G. Pisias, J. D. Hays, J. Imbrie, T. C. Moore, N. J. Shackleton, and Y. Lancelot (1987), Age dating and the orbital theory of ice ages: Development of high resolution 0 to 300,000-year chronostratigraphy, *Quat. Res.*, *27*, 1–29.

Masson, D. G., R. B. Wynn, and B. J. Bett (2004), Sedimentary environment of the Faroe-Shetland and Faroe Bank

Channels, north-east Atlantic, and the use of bedforms as indicators of bottom current velocity in the deep ocean, *Sedimentology*, *51*, 1207–1241.
Mauritzen, C., K. L. Polzin, M. S. McCartney, R. C. Millard, and D. E. West-Mack (2002), Evidence in hydrography and density fine structure for enhanced vertical mixing over the Mid-Atlantic Ridge in the western Atlantic, *J. Geophys. Res.*, *107*(C10), 3147, doi:10.1029/2001JC001114.
McCave, I. N. (1978), Grain size trends and transport along beaches: Example from eastern England, *Mar. Geol.*, *28*, M43–M51.
McCave, I. N. (1983), Particulate size spectra, behavior and origin of nepheloid layers over the Nova Scotian Continental Rise, *J. Geophys. Res.*, *88*, 7647–7666.
McCave, I. N. (1984), Size-spectra and aggregation of suspended particles in the deep ocean, *Deep Sea Res., Part A*, *31*, 329–352.
McCave, I. N. (1985), Stratigraphy and sedimentology of box cores from the HEBBLE site on the Nova Scotian Continental Rise, *Mar. Geol.*, *66*, 59–89.
McCave, I. N. (1988), Biological pumping upwards of the coarse fraction of deep-sea sediments, *J. Sediment. Petrol.*, *58*, 148–158.
McCave, I. N., and L. Carter (1997), Recent sedimentation beneath the Deep Western Boundary Current off northern New Zealand, *Deep Sea Res., Part II*, *44*, 1203–1237.
McCave, I. N., and J. Jarvis (1973), Use of the Model T Coulter Counter in size analysis of fine to coarse sand, *Sedimentology*, *20*, 305–315.
McCave, I. N., and S. A. Swift (1976), A physical model for the rate of deposition of fine-grained sediment in the deep sea, *Geol. Soc. Am. Bull.*, *87*, 541–546.
McCave, I. N., and J. P. M. Syvitski (1991), Principles and methods of geological particle size analysis, in *Principles, Methods and Application of Particle Size Analysis*, edited by J. P. M. Syvitski, pp. 3–21, Cambridge Univ. Press, New York.
McCave, I. N., C. D. Hollister, E. P. Laine, P. F. Lonsdale, and M. J. Richardson (1982), Erosion and deposition on the eastern margin of Bermuda Rise in the Late Quaternary, *Deep Sea Res., Part A*, *29*, 535–561.
McCave, I. N., B. Manighetti, and S. G. Robinson (1995a), Sortable silt and fine sediment size/composition slicing: Parameters for paleocurrent speed and paleoceanography, *Paleoceanography*, *10*, 593–610.
McCave, I. N., B. Manighetti, and N. A. S. Beveridge (1995b), Changes in circulation of the North Atlantic during the last 25,000 years inferred from grain size measurements, *Nature*, *374*, 149–152.
McCave, I. N., T. Kiefer, D. J. R. Thornalley, and H. Elderfield (2005), Deep flow in the Madagascar-Mascarene Basin over the last 150,000 years, *Philos. Trans. R. Soc. London, Ser. A*, *363*(1826), 81–99.
McCave, I. N., I. R. Hall, and G. G. Bianchi (2006), Instrumental differences in silt grain size measurements for estimation of palaeocurrent vigour, *Sedimentology*, *53*, doi:10.1111/j.1365-3091.2006.00783.x.
McLaren, P., and D. Bowles (1985), The effects of sediment transport on grain-size distributions, *J. Sediment. Petrol.*, *55*, 457–470.
McManus, J. F., R. Francois, J.-M. Gherardi, L. D. Keigwin, and S. Brown-Leger (2004), Collapse and rapid resumption of Atlantic meridional circulation linked to deglacial climate changes, *Nature*, *428*, 834–837.
Mehta, A. J., and J. W. Lott (1987), Sorting of fine sediment during deposition, in *Coastal Sediments '87*, vol. I, edited by N. C. Kraus, pp. 348–362, Am. Soc. of Civil Eng., New York.
Menard, H. W., and S. M. Smith (1966), Hypsometry of ocean basin provinces, *J. Geophys. Res.*, *71*, 4305–4325.
Middleton, G. V. (1970), Generation of the log-normal frequency distribution in sediments, in *Topics in Mathematical Geology*, edited by M. A. Romanova and O. V. Sarmanov, pp. 34–42, Consultants Bur., New York.
Miller, M. C., and P. D. Komar (1977), Development of sediment threshold curves for unusual environments (Mars) and for inadequately studied materials (foram sands), *Sedimentology*, *24*, 709–721.
Miller, M. C., I. N. McCave, and P. D. Komar (1977), Threshold of sediment motion under unidirectional currents, *Sedimentology*, *24*, 507–527.
Milligan, T. G., and K. Kranck (1991), Electroresistance particle size analysers, in *Principles, Methods and Application of Particle Size Analysis*, edited by J. P. M. Syvitski, pp. 109–118, Cambridge Univ. Press, New York.
Moreno, E., N. Thouveny, D. Delanghe, I. N. McCave, and N. J. Shackleton (2002), Climatic and oceanographic changes in the northeast Atlantic reflected by magnetic properties of sediments deposited on the Portuguese margin during the last 340 ka, *Earth Planet. Sci. Lett.*, *202*, 465–480.
Nezu, I., and H. Nakagawa (1993), *Turbulence in Open-Channel Flows*, Int. Assoc. Hydraul. Res. Monogr., A. A. Balkema, Brookfield, Vt.
North Greenland Ice Core Project Members (2004), High-resolution record of Northern Hemisphere climate extending into the last interglacial period, *Nature*, *431*, 147–151.
O'Brien, S. R., P. A. Mayewski, L. D. Meeker, D. A. Meese, M. S. Twickler, and S. I. Whitlow (1995), Complexity of Holocene climate as reconstructed from a Greenland ice core, *Science*, *270*, 1962–1964.
Pascoe, G. A., P. McLaren, and M. Soldate (2002), Impact of offsite sediment transport and toxicity on remediation of a contaminated estuarine bay, *Mar. Pollut. Bull.*, *44*, 1184–1193.
Passega, R. (1957), Texture as characteristic of clastic deposition, *Am. Assoc. Petrol. Geol. Bull.*, *41*, 1952–1984.
Paull, C. K., S. J. Hills, and H. R. Thierstein (1988), Progressive dissolution of fine carbonate particles in pelagic sediments, *Mar. Geol.*, *81*, 27–40.
Pfuhl, H. A., and I. N. McCave (2005), Evidence for late Oligocene establishment of the Antarctic Circumpolar Current, *Earth Planet. Sci. Lett.*, *235*, 715–728.
Piotrowski, A. M., S. L. Goldstein, S. R. Hemming, and R. G. Fairbanks (2004), Intensification and variability of ocean thermohaline circulation through the last deglaciation, *Earth Planet. Sci. Lett.*, *225*, 205–220.
Polzin, K. L., J. M. Toole, J. R. Ledwell, and R. W. Schmitt (1997), Spatial variability of turbulent mixing in the abyssal ocean, *Science*, *276*, 93–96.
Potter, P. E., D. Heling, N. F. Shimp, and W. VanWie (1975), Clay mineralogy of modern alluvial muds of the Mississippi River Basin, *Bull. Cent. Rech. Pau-SNPA*, *9*, 353–389.
Prins, M. A., and G. J. Weltje (1999), End-member modeling of siliciclastic grain-size distributions: The Late Quaternary record of eolian and fluvial sediment supply to the Arabian Sea and its paleoclimatic significance, *SEPM Spec. Publ.*, *62*, 91–111.
Prins, M. A., L. M. Bouwer, C. J. Beets, S. R. Troelstra, G. J. Weltje, R. W. Kruk, A. Kuijpers, and P. Z. Vroon (2002), Ocean circulation and iceberg discharge in the glacial North

Atlantic: Inferences from unmixing of sediment size distributions, *Geology*, *30*, 555–558.
Pudsey, C. J., and J. A. Howe (1998), Quaternary history of the Antarctic Circumpolar Current: Evidence from the Scotia Sea, *Mar. Geol.*, *148*, 83–112.
Rahmstorf, S., and M. H. England (1997), Influence of southern hemisphere winds on North Atlantic Deep Waterflow, *J. Phys. Oceanogr.*, *27*, 2040–2054.
Raymo, M. E., W. F. Ruddiman, N. J. Shackleton, and D. W. Oppo (1990), Evolution of Atlantic-Pacific $\delta^{13}C$ gradients over the last 2.5 m. y., *Earth Planet. Sci. Lett.*, *97*, 353–368.
Raymo, M. E., D. E. Oppo, and W. Curry (1997), The mid-Pleistocene climate transition: A deep sea carbon isotopic perspective, *Paleoceanography*, *12*, 546–559.
Rees, A. I. (1961), The effect of water currents on the magnetic remanence and anisotropy of susceptibility of some sediments, *Geophys. J. R. Astron. Soc.*, *5*, 235–251.
Revel, M., M. Cremer, F. E. Grousset, and L. Labeyrie (1996), Grain-size and Sr-Nd isotopes as tracers of paleo-bottom current strength, northeast Atlantic Ocean, *Mar. Geol.*, *131*, 233–249.
Richardson, M. J., G. L. Weatherly, and W. D. Gardner (1993), Benthic storms in the Argentine Basin, *Deep Sea Res., Part II*, *40*, 975–987.
Risebrobakken, B., E. Jansen, C. Andersson, E. Mjelde, and K. Hevrøy (2003), A high-resolution study of Holocene paleoclimatic and paleoceanographic changes in the Nordic Seas, *Paleoceanography*, *18*(1), 1017, doi:10.1029/2002PA000764.
Robinson, S. G., and I. N. McCave (1994), Orbital forcing of bottom-current enhanced sedimentation on Feni Drift, N. E. Atlantic, during the mid-Pleistocene, *Paleoceanography*, *9*, 943–972.
Rosin, P., and E. Rammler (1933), Laws governing the fineness of powdered coal, *J. Inst. Fuel*, *7*, 29–36.
Russel, W. B. (1980), Review of the role of colloidal forces in the rheology of suspensions, *J. Rheol.*, *24*, 287–317.
Schaaff, E., C. Grenz, C. Pinazo, and B. Lansard (2006), Field and laboratory measurements of sediment erodibility: A comparison, *J. Sea Res.*, *55*, 30–42.
Schulz, M., and A. Paul (2002), Holocene climate variability on centennial-to-millennial time scales: 1. Climate records from the North-Atlantic realm, in *Climate Development and History of the North Atlantic Realm*, edited by G. Wefer et al., pp. 41–54, Springer, New York.
Self, R. F. L., A. R. M. Nowell, and P. A. Jumars (1989), Factors controlling critical shears for deposition and erosion of individual grains, *Mar. Geol.*, *86*, 181–199.
Sheldon, R. W., and T. R. Parsons (1967), *A Practical Manual on the Use of the Coulter Counter in Marine Science*, 66 pp., Coulter Electron. Sales Co., Toronto, Canada.
Siddall, M., E. J. Rohling, A. Almogi-Labin, C. Hemleben, D. Meischner, I. Schmelzer, and D. A. Smeed (2003), Sea-level fluctuations during the last glacial cycle, *Nature*, *423*, 853–858.
Singer, J., J. B. Anderson, M. T. Ledbetter, K. P. N. Jones, I. N. McCave, and R. Wright (1988), The assessment of analytical techniques for the analysis of fine-grained sediments, *J. Sediment. Petrol.*, *58*, 534–543.
Snowball, I., and M. Moros (2003), Saw-tooth pattern of North Atlantic current speed during Dansgaard-Oeschger cycles revealed by the magnetic grain size of Reykjanes Ridge sediments at 59°N, *Paleoceanography*, *18*(2), 1026, doi:10.1029/2001PA000732.
Stein, R. (1985), Rapid grain-size analysis of silt and clay fraction by Sedigraph 5000D: Comparison with Coulter Counter and Atterberg methods, *J. Sediment. Petrol.*, *55*, 590–615.
Stickley, C. E., L. Carter, I. N. McCave, and P. P. E. Weaver (2001), Variations in the CDW flow through the SW Pacific gateway for the last 190 ky: Evidence from Antarctic diatoms, in *The Oceans and Rapid Climate Change: Past, Present, and Future*, *Geophys. Monogr. Ser.*, vol. 126, edited by D. Seidov et al., pp. 101–116, AGU, Washington, D. C.
Stickley, C. E., H. Brinkhuis, S. A. Schellenberg, A. Sluijs, U. Röhl, M. Fuller, M. Grauert, M. Huber, J. Warnaar, and G. L. Williams (2004), Timing and nature of the deepening of the Tasmanian Gateway, *Paleoceanography*, *19*, PA4027, doi:10.1029/2004PA001022.
Stow, D. A. V., J.-C. Faugeres, J. A. Howe, C. J. Pudsey, and A. R. Viana (2002), Bottom currents, contourites and deep-sea sediment drifts: Current state-of-the-art, in *Deep-Water Contourite Systems: Modern Drifts and Ancient Series, Seismic and Sedimentary Characteristics*, *Geol Soc. London Mem.*, vol. 22, edited by Stow et al., pp. 7–20, Geol. Soc. of London, London.
Stuiver, M., and T. F. Braziunas (1989), Atmospheric ^{14}C and century-scale solar oscillations, *Nature*, *338*, 404–408.
Stuut, J.-B. W., M. A. Prins, R. R. Schneider, G. J. Weltje, J. H. F. Jansen, and G. Postma (2002), A 300 kyr record of aridity and wind strength in southwestern Africa: Inferences from grain-size distributions of sediments on Walvis Ridge, SE Atlantic, *Mar. Geol.*, *180*, 221–233.
Sun, D., J. Bloemendal, D. K. Rea, J. Vandenberghe, F. Jiang, Z. An, and R. Su (2002), Grain-size distribution function of polymodal sediments in hydraulic and aeolian environments, and numerical partitioning of the sedimentary components, *Sediment. Geol.*, *152*, 263–277.
Sundborg, A. (1956), The River Klaralven, a study of fluvial processes, *Geogr. Ann.*, *38*, 125–316.
Syvitski, J. P. M., K. W. G. LeBlanc, and K. W. Asprey (1991), Interlaboratory, interinstrument calibration experiment, in *Principles, Methods and Application of Particle Size Analysis*, edited by J. P. M. Syvitski, pp. 174–193, Cambridge Univ. Press, New York.
Thomsen, L. (2005), Organic rich aggregates in the ocean: Formation, transport behavior, and biochemical composition, in *Flocculation in Natural and Engineered Environmental Systems*, edited by I. G. Droppo et al., pp. 237–248, CRC Press, Boca Raton, Fla.
Trentesaux, A., P. Recourt, V. Bout-Roumazeilles, and N. Tribovillard (2001), Carbonate grain-size distribution in hemipelagic sediments from a laser particle sizer, *J. Sediment. Res.*, *71*, 858–862.
Tucholke, B. E. (1975), Sediment distribution and deposition by the Western Boundary Undercurrent: The Greater Antilles Outer Ridge, *J. Geol.*, *83*, 177–207.
Tucholke, B. E., and R. W. Embley (1984), Cenozoic regional erosion of the abyssal sea floor off South Africa, *AAPG Mem.*, *35*, 145–164.
Tucholke, B. E., C. D. Hollister, P. E. Biscaye, and W. D. Gardner (1985), Abyssal current character determined from sediment bedforms on the Nova Scotian continental rise, *Mar. Geol.*, *66*, 43–47.
Turcotte, D. L. (1997), *Fractals and Chaos in Geology and Geophysics*, 2nd ed., 398 pp., Cambridge Univ. Press, New York.
Unsold, G. (1982), Der Transportbeginn rolligen Sohlmaterials in gleichformigen turbulenten Stromungen: Eine kritische Uberprüfung der Shields-Funktion und ihre experimentelle

Erweiterung auf feinstkörnige, nicht-bindige Sedimente, doctoral dissertation, 145 pp., Univ. of Kiel, Kiel, Germany.

Wang, H., and I. N. McCave (1990), Distinguishing climatic and current effects in mid-Pleistocene sediments of Hatton and Gardar Drifts, N. E. Atlantic, *J. Geol. Soc. London*, *147*, 373–383.

Warren, B. A., T. Whitworth, and J. H. LaCasce (2002), Forced resonant undulation in the deep Mascarene Basin, *Deep Sea Res., Part II*, *49*, 1513–1526.

Weaver, C. E. (1989), *Clays, Muds and Shales*, 810 pp., Elsevier, New York.

Weaver, P. P. E., and J. Thomson (1993), Calculating erosion by deep-sea turbidity currents during initiation and flow, *Nature*, *364*, 136–138.

Weber, O., E. Gonthier, and J.-C. Faugères (1991), Analyse granulometrique de sediments fins marins: Comparaison des resultats obtenus au Sedigraph et au Malvern, *Bull. Inst. Géol. Bassin Aquitaine*, *50*, 107–114.

Weltje, G. J. (1997), End-member modeling of compositional data: Numerical-statistical algorithms for solving the explicit mixing problem, *Math. Geol.*, *29*, 503–549.

Weltje, G. J., and M. A. Prins (2003), Muddled or mixed? Inferring palaeoclimate from size distributions of deep-sea clastics, *Sediment. Geol.*, *162*, 39–62.

Winterwerp, J. C., and W. G. M. van Kesteren (2004), *Introduction to the Physics of Cohesive Sediment in the Marine Environment*, 466 pp., Elsevier, New York.

Wunsch, C. (2000), On sharp spectral lines in the climate record and the millennial peak, *Paleoceanography*, *15*, 417–424.

Xu, R. (2000), *Particle Characterization: Light Scattering Methods*, 397 pp., Springer, New York.

Yokokawa, M., and S. O. Franz (2002), Changes in grain size and magnetic fabric at Blake-Bahama Outer Ridge during the late Pleistocene (marine isotope stages 8–10), *Mar. Geol.*, *189*, 123–144.